







Article

Assessing Nitrogen Dioxide in the Highveld Troposphere: Pandora Insights and TROPOMI Sentinel-5P Evaluation

Refilwe F. Kai-Sikhakhane ^{1,*}, Mary C. Scholes ¹, Stuart J. Piketh ², Jos van Geffen ³, Rebecca M. Garland ⁴, Henno Havenga ² and Robert J. Scholes ^{5,†}

¹ School of Animal, Plant and Environmental Sciences, University of the Witwatersrand, Johannesburg 2001, South Africa; mary.scholes@wits.ac.za

² Unit for Environmental Sciences and Management, North-West University, Potchefstroom 2531, South Africa; stuart.piketh@nwu.ac.za (S.J.P.); henno.havenga@nwu.ac.za (H.H.)

³ Royal Netherlands Meteorological Institute (KNMI), P.O. Box 201, 3730 AE De Bilt, The Netherlands; jos.van.geffen@knmi.nl

⁴ Department of Geography, Geoinformatics and Meteorology, University of Pretoria, Pretoria 0028, South Africa; rebecca.garland@up.ac.za

⁵ Global Change Institute, University of the Witwatersrand, Johannesburg 2001, South Africa

* Correspondence: 741786@students.wits.ac.za

† Deceased author.

Abstract: Nitrogen oxides, particularly NO₂, are emitted through a variety of industrial and transport processes globally. The world's continuous economic development, including in developing countries, results in an increasing concentration of those gases in the atmosphere. Yet, there is scant information on the current state and recent evolution of these atmospheric pollutants over a range of spatial and temporal scales, especially in Africa. This, in turn, hinders the assessment of the emissions and the evaluation of potential risks or impacts on societies and their economies, as well as on the environment. This study attempts to fill the gap by leveraging data from a Pandora-2S ground-based, column-integrating instrument located in Wakkerstroom in the Mpumalanga Province of South Africa and space-based remote sensing data obtained from the TROPOMI instrument onboard the ESA Sentinel-5P satellite. We compare these two spatially (horizontal) representative data sets using statistical tools to investigate the concentrations of emitted and transported NO₂ at this particular location, expecting that a significant positive correlation between the NO₂ tropospheric vertical column (TVC) data might justify using the TROPOMI data, available globally, as a proxy for tropospheric and boundary layer NO₂ concentrations over the Highveld of South Africa more generally. The data from the two instruments showed no significant difference between the interannual mean TVC-NO₂ in 2020 and 2021. The seasonal patterns for both instruments were different in 2020, but in 2021, both measured peak TVC-NO₂ concentrations in late winter (week 34). The instruments both detected higher TVC-NO₂ concentrations during transitions between seasons, particularly from winter to spring. The TVC-NO₂ concentrations measured in Wakkerstroom Mpumalanga are mostly contributed to by the emission sources in the low troposphere, such as biomass burning and emissions from local power stations.

Keywords: Pandora-2s; nitrogen dioxide; TROPOMI; Sentinel-5P; air quality; validation



Citation: Kai-Sikhakhane, R.F.; Scholes, M.C.; Piketh, S.J.; van Geffen, J.; Garland, R.M.; Havenga, H.; Scholes, R.J. Assessing Nitrogen Dioxide in the Highveld Troposphere: Pandora Insights and TROPOMI Sentinel-5P Evaluation. *Atmosphere* **2024**, *15*, 1187. <https://doi.org/10.3390/atmos15101187>

Academic Editor: David F Plusquellic

Received: 5 August 2024

Revised: 23 September 2024

Accepted: 27 September 2024

Published: 3 October 2024



Copyright: © 2024 by the authors. Licensee MDPI, Basel, Switzerland. This article is an open access article distributed under the terms and conditions of the Creative Commons Attribution (CC BY) license (<https://creativecommons.org/licenses/by/4.0/>).

1. Introduction

Developing countries contribute increasing amounts of pollution to the atmosphere [1,2], adding to the existing burden of air pollution from developed countries. In the United Kingdom (UK), nitrogen oxide (NO_x) emissions totalled 6433 tonnes in 2022 and 6.1 million tonnes in the United States of America (US) in 2023 [3]. The presence of NO_x in the atmosphere, particularly the lower troposphere, is detrimental to the environment (e.g., acidic deposition) and has negative health impacts, including cardiovascular and

respiratory diseases [4–7]. The World Health Organization (WHO) reports that pollutants such as particulate matter (PM), carbon monoxide (CO), ozone (O₃), nitrogen dioxide (NO₂) and sulphur dioxide (SO₂) show the most evidence of having an impact on public health, in addition to any environmental impacts. The distribution patterns of these pollutants differ, with NO₂ showing a distinct urban-rural gradient of higher concentrations in more densely populated urban areas [8] and highly industrialised regions [9]. The only way to minimise these impacts is to regulate the emissions into the atmosphere [10].

Nitrogen dioxide (NO₂) is the most prevalent form of NO_x in the atmosphere. Anthropogenic activities such as biomass burning, incomplete combustion of coal (power generation) and transport lead to the generation of NO [10], which is then rapidly converted to NO₂ [11]. During the day, the formation of NO₂ is favoured, which then catalyses the formation of nitric acid (HNO₃). At night, ozone reacts with NO₂ to yield reactive nitrogen in the form of nitrate (NO₃[−]) [12]. Reactive nitrogen is removed from the atmosphere through wet or dry deposition in the environment, contributing to the nitrogen status of terrestrial and aquatic ecosystems [13]. Studies show that South Africa's highly industrialised Highveld area has high tropospheric NO₂ concentrations, exceeding the national air quality standards [14]. These elevated concentrations are comparable to those of severely polluted regions of North America and Southeast Asia (between 1.30×10^{-4} and 3.72×10^{-4} mol/m²) [4,15].

Consequently, cities near the industrialised Highveld, such as Johannesburg, experience higher annual NO₂ column concentrations than coastal cities away from the Highveld [16]. NO_x emissions reported in the South African Mpumalanga (MP) Highveld are dominated by those emanating from coal-fired power stations and industrial activities [17,18] and contribute to the observed high levels of tropospheric NO₂ [4,7]. In addition to coal-burning power stations, other significant emission contributions to the Highveld tropospheric NO₂ column concentrations include biomass burning (particularly in the austral spring), the transport sector, and wood burning from informal household cooking and heating [16,19]. Power station emissions in the MP Highveld occur at ca. 250 m above the surface [20] and rise to altitudes of 500 m to 1000 m due to their heat content but are mixed downwards to the surface due to vertical mixing in the boundary layer under high solar radiation conditions [21]. These tropospheric pollutants are subjected to chemical and physical processes, which are highly dependent on meteorological conditions, resulting in their dispersion and transport [22].

The literature shows that NO_x concentrations in the Highveld of South Africa peak diurnally at midday [14]. These peaks can be influenced by transboundary transported emissions [16], depending on the air mass' long- and short-range transport over the Mpumalanga Highveld. According to Freiman and Piketh [23], four major pollution transport pathways to the Highveld have been identified, depending on the source regions. Airflow to the region is driven by pathways from subtropical Africa, the Atlantic and the Indian Oceans, and flow over southern Africa. Emissions in the Highveld are recirculated or transported out of the region into the south Indian Ocean [23].

However, since temporally and spatially resolved instruments for trace gas monitoring are still sparse in Africa [24], we are faced with an incomplete understanding of the atmospheric chemistry in the tropospheric and total column. The available data in Africa, usually scanty in comparison to the northern hemisphere, is from campaigns testing novel technologies for a short period [25]. The transport of pollutants from neighbouring countries into South Africa can be documented using satellite remote sensing data combined with atmospheric circulation information generated by weather forecasting models [7,26,27].

There is a rich legacy of monitoring atmospheric NO₂ global distributions using remote sensing. From the late 1970s, limb-viewing and solar-occultation instruments were used [28,29]. However, these instruments have been replaced with satellites with higher spatial resolution, and improved retrieval methods have been implemented. The Tropospheric Monitoring Instrument (TROPOMI), on board the European Space Agency (ESA)

Sentinel-5 Precursor (S5P) payload, has a higher spatial resolution than its predecessor, the Ozone Monitoring Instrument (OMI). This feature, in turn, allows the documentation of NO_x emissions in individual cities and effectively identifies NO₂ hotspots [30]. Scientific investigations and accumulated expertise have shown that satellite data can be combined effectively with atmospheric circulation models and knowledge about chemical reactions to detect and monitor highly polluted areas against the prevailing background values.

TROPOMI uses the differential optical absorption spectroscopy (DOAS) technique to quantify the total trace gas amount along the effective light path from the sun through the atmosphere to the instrument [31]. TROPOMI produces high-resolution data ($\sim 5.5 \times 3.5 \text{ km}^2$) [31] for the UV-Vis spectral range. This instrument is able to yield near-global measurements daily due to its 2600 km swath [31].

The proper interpretation of TROPOMI data requires a deep understanding of the transfer of solar radiation in the atmosphere, particularly the specific absorption bands of atmospheric NO₂ pollutants. Such a radiation model can be inverted against satellite data, and the latter can be used to document the spatial and temporal distribution of those NO₂ trace gases over the area of interest. This process, therefore, also requires prior knowledge of the underlying topography to determine the true extent of the slanted atmospheric columns in which radiation scattering and absorption are taking place for each grid cell of the satellite data [32,33].

The quantitative information retrieved from the satellite data can be compared subsequently with the independently acquired data from ground-based measurements, such as Pandora instruments [34], paying particular attention to the differences in spatial, temporal, and accuracy characteristics of those instruments. Due to TROPOMI's global coverage, it lacks temporal resolution. Therefore, data from ground-based instruments such as Pandora complement these high-quality, spatially resolved satellite data products.

Ground instruments can capture localised measurements, enabling researchers to study events at specific locations using high temporal resolution. The ability of ground-based instruments to vertically profile the measured trace gases in the atmosphere allows access to the integrated vertical profile concentrations from the satellite-derived measurements. Not only is it important to understand the horizontal distribution of NO₂ across the globe, but the vertical distribution is extremely important as it identifies the high-impact layers that impact atmospheric chemistry and environmental and health impacts.

Pandora instruments employ direct sun (DS) and multi-axis differential optical absorption spectroscopy (MAX-DOAS) techniques to measure atmospheric trace gas amounts [35]. The DS technique quantifies trace gas abundances in the atmospheric total column (TC) by using scattered light received from one viewing direction at a time: the sun. However, the MAX-DOAS technique uses scattered light from multiple viewing directions and angles. When using the standard Pandora routines for DS measurement, the instrument points directly at the sun for approximately 60 s at a time. For MAX-DOAS measurements, the instrument scans the sky at various elevation angles for a fixed pointing azimuth (PAZI) for 30 s per angle. The MAX-DOAS technique is more sensitive to atmospheric constituents abundant in the lower troposphere, such as NO₂. Literature shows that a detailed evaluation of satellite-derived NO₂ concentrations using ground-based instruments has been carried out using DS measurements since they are more vertically representative of the satellite-derived measurements. These evaluations show that TROPOMI underestimates NO₂ tropospheric vertical column (TVC) concentrations [1,29,36]. The global negative biases observed between TROPOMI and MAX-DOAS measurements are reported as high as 37% in clean to slightly polluted areas and can increase to 51% in highly polluted areas [29]. These biases differ by region and specific ground-based stations. The measurement biases observed are attributable to the different viewing geometries between these two instruments, biases in the satellite retrieval of cloud pressure, the surface albedo climatology, and the low resolution of the a priori profiles derived from global simulations of the TM5-MP chemistry model [29,37,38]. Duoros et al. [28] showed that replacing the global a priori information with local a priori information decreased the overall bias by 5% to

12%. Additionally, DS measurements are not horizontally representative of the TROPOMI footprint because measurements are taken at one point, and the field of view of the Pandora instrument is small, $\sim 1.5^\circ$.

Dimitriopoulou et al. [39] show that using MAX-DOAS instruments to measure tropospheric NO_2 concentrations in different directions improves the spatial collocation of ground-derived measurements with satellite-derived measurements. In addition, the Pandora instrument's temporal resolution can capture the NO_2 diurnal variation that isn't captured by satellite measurements due to the polar-orbiting nature of the satellite instrument [4].

Since Pandora TVC measurements can be retrieved at very high temporal frequency, it is possible to select the values corresponding to the time of passage of TROPOMI over an area of interest and compare data sets acquired quasi simultaneously. A reasonable comparison between the TROPOMI- and Pandora-derived MAX-DOAS measurements can indicate the balancing association of these two datasets, indicating the need for ground instruments to supplement the temporally lacking, column-integrated TROPOMI measurements.

This study evaluates the heterogeneity of the TVC- NO_2 concentrations over Wakkerstroom in the Mpumalanga Highveld region of South Africa using Pandora, now known as Pan159, MAX-DOAS measurements. In addition, the TROPOMI-derived TVC measurements are presented and evaluated alongside the Pandora-derived measurements. The purpose of this comparison is to assess whether or not the TROPOMI data can be used as a reliable proxy for the tropospheric and boundary layer concentrations of NO_2 of the South African Highveld, a hotspot of emissions at a global scale.

2. Materials and Methods

2.1. Study Site Description

Wakkerstroom ($27^\circ 21' 17.7''$ S, $30^\circ 08' 37.8''$ E) is located in the Mpumalanga Province of South Africa (Figure 1). The town covers an area of 87.68 km^2 , with a population of ~ 7000 and a minimum elevation of approximately 1730 m a.s.l. The study site is relatively close to 12 coal-fired power stations (within $\sim 48 \text{ km}$ to 214 km). The power stations in the Highveld are direct emission sources of NO_x . Wakkerstroom is downwind of the majority of the power stations. The closest power stations to Wakkerstroom are Majuba and Camden. Camden is located northeast, while Majuba is located northwest of Wakkerstroom. The NO_x agricultural emissions from neighbouring townships and surrounding agricultural areas also increase the pollution load in the atmosphere [40]. As a result of this concentration of power stations, the Highveld has long been identified as a major source of NO_2 pollution, even on a subcontinental scale (Figure 2).

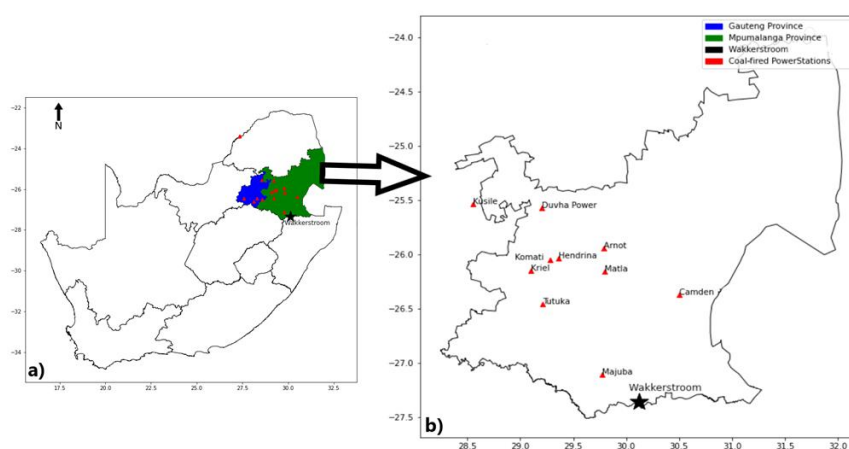


Figure 1. Map of South Africa depicting the (a) Mpumalanga (MP) and Gauteng (GP) Provinces with (b) the Mpumalanga Province of South Africa showing the coal-fired power stations in the MP

Highveld and Wakkerstroom where the Pandora instrument (Pan159) is situated. Source of shapefiles: <https://www.igismap.com/south-africa-shapefile-download-boundary-line-polygon/> (accessed on 11 December 2022).

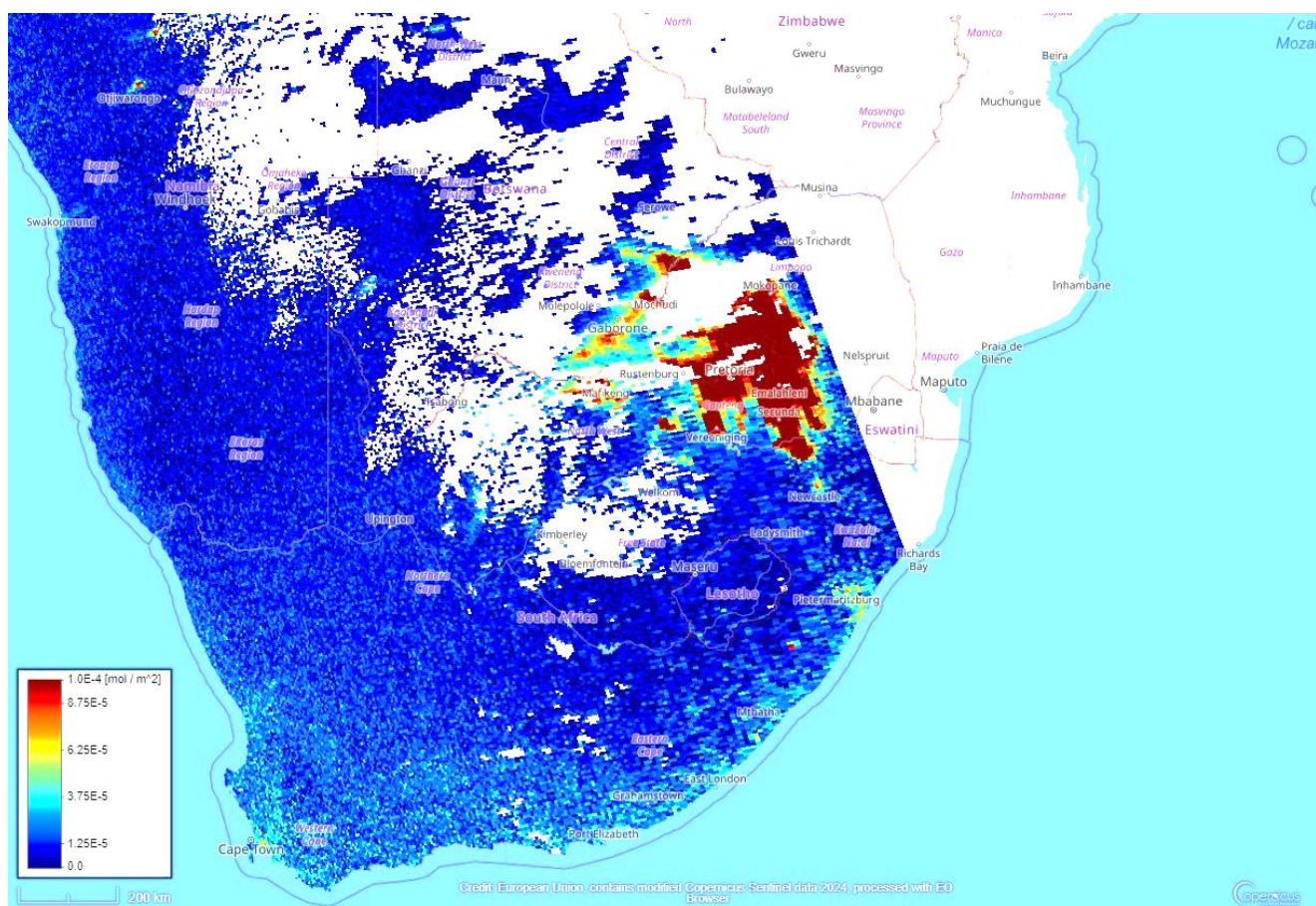


Figure 2. Map of the tropospheric column NO₂ concentrations (mol/m²) over southern Africa, as derived from an analysis of TROPOMI data from the 7–20 June 2021. Source: <https://browser.dataspace.copernicus.eu/> (accessed on 26 September 2024).

2.2. Research Techniques and Methods

2.2.1. Pandora-2s Instrument

The Pandora instrument installed in Wakkerstroom is part of the ground-based standardised Pandora sun photometer network (Pandora Global Network-PGN). The Pandora-2Spectrometer (2s) instrument is a dual ultraviolet (UV) and visible (VIS) spectrometer system that delivers integrated column direct sun/moon and sky-scanned observations of various trace gases, including O₃, NO₂, SO₂, and CH₂O [41]. It is also possible to derive an atmospheric profile of the selected trace gases. This device is a small, cost-effective instrument capable of providing high-precision observations from 280 nm to 530 nm. The Pandora instrument used in this study (Pan159) was deployed in Wakkerstroom in December 2019. It has a spectral range of 270 nm to 530 nm and 400 nm to 900 nm and a resolution of 0.6 nm/UV and 1.1 nm/VIS. The Pandora-2s is mounted on an azimuth and elevation tracker that is controlled by a microprocessor (https://sciglob.com/wp-content/uploads/2023/12/Pandora2S_datasheet-1.pdf (accessed on 15 July 2021), making it possible to point the instrument in any direction.

Trace gases absorb solar radiation at specific wavelengths in the ultraviolet to visible spectrum range, resulting in spectral signatures [42]. Trace gas concentrations can, therefore, be determined by measuring their specific spectral signatures using the differential optical absorption spectroscopy (DOAS) method. The DOAS method is used to determine

atmospheric trace gas concentrations from direct sun DOAS (DS-DOAS) observations, multi-axis DOAS (MAX-DOAS), or both. It is possible to repeat the measurements every 80 s. The measured scattered sunlight spectra are analysed using “L2 direct” and “L2 Air-Ratio Sky” algorithms, respectively [43]. The latter algorithm compares observed and reference spectra to determine concentration profiles of atmospheric trace gases [43].

The DS-DOAS technique delivers total column trace gas amounts using direct sun (DS) geometry, which means that it points directly at the sun when measuring spectral signatures of the trace gases. The MAX-DOAS technique, an extension of the traditional DOAS method, scans the sky at various elevations and azimuth angles. This allows for the quasi-simultaneous observation of scattered light in different line-of-sight (LOS) directions from the horizon to the zenith, depending on the sun’s position during observations [44]. The various elevation angles enable measurements at different horizontal distances and provide sensitivity to different atmospheric altitudes. Lower elevation angles are more sensitive to the lower atmosphere because the path length of light is longer in the low troposphere than at higher altitudes. The longer light path length enhances atmospheric constituents’ light absorption, increasing sensitivity to trace gases primarily found in the lower troposphere, such as NO₂, O₃, and CH₂O. As a result, the MAX-DOAS data are only measured in the lower troposphere, up to approximately 5.5 km above ground level [45].

2.2.2. Pandora (Pan159) Data

The Pandora instrument at Wakkerstroom, Pan159, uses both DOAS techniques to measure the concentrations of NO₂, O₃, SO₂, and CH₂O. During the setup of the Pandora instruments for MAX-DOAS measurements, one to three pointing azimuth (PAZI) directions were selected: one direction over the more polluted area and another in the opposite direction. Pan159 was set at a 270° PAZI (west), which looks across the vlei (valley) to the neck of the Volksrust road. Volksrust is a town approximately 45 km from Wakkerstroom and serves as a stopover for travellers commuting between Johannesburg and Durban. Therefore, the set azimuth for Pan159 is in the direction of expected pollution relative to its location. The sky scans are detailed or quick and use an open-hole or a U340 filter. Measurements from detailed sky scan zenith angles [0, 40, 50, 60, 70, 75, 80, 82, 85, “MAX-2”, “MAX-1”, “MAX”, “MAX-1”, “MAX-2”, 85, 82, 80, 75, 70, 60, 50, 40, 0] and quick sky scan elevation angles [0, 60, 75, “MAX-1”, “MAX”, “MAX-1”, 75, 60, 0] using a U340 filter were taken for a total of 30 s at each position; each position is scanned twice for 15 s. Pan159 employs an open-hole filter for quick scans at 0, 60, 75, “MAX-1”, “MAX”, “MAX-1”, 75, 60 and 0-degree zenith angles also for a total of 30 s. Therefore, the measurement frequency is approximately 13 min, depending on the routine schedule and sun searches for the DS measurements. The maximum angle (MAX) was set at 88° as this is the maximum angle of unobstructed view that the instrument can point and measure. The Pan159 angles determine the atmospheric vertical distance that the instrument can sample during measurements. The Pandora instrument in MAX-DOAS mode measures trace gases in the lower troposphere, where the majority of the significant trace gases are concentrated in the atmosphere. At higher altitudes, the signal-to-noise ratio of the trace gas measurements decreases because of the reduced air density and scattering effects. Therefore, Pandora MAX-DOAS measurements are optimised in the lower troposphere only. This study analyses the tropospheric vertical column (TVC) NO₂ concentrations (mol/m²) from 2020 to 2021.

The quasi-continuous Pan159 data are assigned data quality flag (DQF) values to qualify their uncertainty and usability; see Table 1. Pandora level 2 (L2) data quality flags are discussed in [45]. This study uses high-quality data with DQFs of 0/10 only.

Table 1. Pandora instrument data quality flags (DQFs) and their meanings.

| Data Quality Flag (DQF) Value | Explanation |
|-------------------------------|---|
| 0 | High-quality data (quality assurance applied) |
| 1 | Medium-quality data (quality assurance applied) |
| 2 | Low-quality data (quality assurance applied) |
| 10 | High-quality data (quality assurance not applied) |
| 11 | Medium-quality data (quality assurance not applied) |
| 12 | Low-quality data (quality assurance not applied) |
| 20 | Unusable data |
| 21 | Unusable data |
| 22 | Unusable data |

2.2.3. TROPOMI Instrument

The TROPospheric Monitoring Instrument (TROPOMI) is a sensor aboard the European Space Agency's (ESA's) polar-orbiting Sentinel-5 Precursor (S5P) satellite [31,46]. It was launched in 2017 to provide atmospheric trace gas, cloud and aerosol property measurements using shortwave infrared (SWIR), near-infrared (NIR), ultraviolet (UV) and visible (VIS) spectroscopy [31] from an ascending sun-synchronous polar orbit, with the equator crossing about 13:30 local time at the location of overpass [31]. The solar radiation is measured within the 405 nm to 465 nm wavelength range, and retrieval algorithms are used to derive the tropospheric NO₂ column density at $\sim 5.5 \times 3.5$ km² spatial resolution from August 2019 [47]. The first public release of TROPOMI data sets, including NO₂, was in July 2018 [31,48]. The offline (OFFL) level-2 (L2) tropospheric NO₂ column density data can currently be accessed via the Copernicus Data Space Ecosystem (CDSE; <https://dataspace.copernicus.eu/>, last accessed on 21 June 2022). The S5P data processor has been upgraded since the start of the mission. With respect to NO₂ column amounts, the measurement process starts with the retrieval of slant column densities (SCDs). This is followed by separating the total SCDs into stratospheric and tropospheric components, depending on a priori vertical profile information using air-mass factors (AMFs), considering atmospheric cloud cover. The correct interpretation of TROPOMI data requires an understanding of the transfer of solar radiation in the atmosphere, particularly the specific absorption bands of the NO₂ pollutants.

2.2.4. TROPOMI Data

This study used NO₂ data product version 2.4.0 [31,48,49] from January 2020 to December 2021. The TROPOMI satellite output for each ground pixel, including the TVC-NO₂ concentrations measured in the visible spectral range, was assigned a quality indicator, "quality assurance value", to indicate the quality of the retrieved trace gas amount [31]. Pixel output with qa-value ≥ 0.75 are expected to originate from cloud-free areas and are considered error-free [48] and are used in this study. The original TROPOMI data were re-gridded to 0.01°, allowing us to select an area around Wakkerstroom that is representative of the area measured by the Pandora instrument using MAX-DOAS. A 0.1° \times 0.05° area around Wakkerstroom was selected and averaged. The non-normally distributed data were averaged weekly, and the means, medians and standard deviations (variations) are reported in this study.

2.2.5. Data Evaluation

The traditional evaluation method [1,50] applied in this study used Pandora-2s tropospheric NO₂ concentrations (1) \pm 5 min of the TROPOMI overpass time and (2) an hour within the TROPOMI overpass time for analyses. For the purpose of this study, only data from the TROPOMI pixel closest to the Wakkerstroom site were extracted.

All TROPOMI data used to compute the regression statistics were of qa-values ≥ 0.75 , and the Pandora data were of DQF 0 or 10. In general, the use of TROPOMI data with qa-values ≥ 0.75 excludes data observed over cloudy scenes (cloud radiance fraction > 0.5), scenes covered by snow/ice, and retrievals considered unreliable for any number of reasons. The ± 5 min Pandora coincidence measurements were 5 min before or after the TROPOMI overpass time. The 1 h coincidence measurements were Pandora measurements retrieved within the TROPOMI overpass hour. These measurements were averaged and used as the 1 h coincidence data.

Theil Sen regression analyses (Rstudio[®]) were used to compute all the regression statistics (R; *p*-value and regression line), Equation (1) was applied to compute the normalised mean bias (NMB), and Equation (2) for the NMB percentage. The Relative Squared Errors (RSEs) for all the regressions were computed to validate the regression models in this study.

$$\text{Normalised Mean Bias} = \frac{\sum_1^n (M - O)}{\sum_1^n (O)} \quad (1)$$

$$\text{Normalised Mean Bias (\%)} = \frac{\sum_1^n (M - O)}{\sum_1^n (O)} \times 100 \quad (2)$$

O = Pandora-2s measurements M = TROPOMI measurements.

2.2.6. A Priori Profiles Data

The NO₂ profiles (a priori profile shapes) were extracted from the TM5-MP (Tracer Model, version 5), a chemistry-transport model employed to derive highly resolved vertical profiles of NO₂ and other trace gases used in satellite retrievals [51]. The profiles were extracted using the Python tool developed by the Koninklijk Nederlands Meteorologisch Instituut (KNMI). The .py code for the auxiliary product can be accessed from the Product User Manual (see <https://sentinel.esa.int/web/sentinel/user-guides/sentinel-5p-tropomi/software-tools> (accessed on 10 November 2022)).

2.2.7. Hybrid Single-Particle Lagrangian Integrated Trajectory (HYSPLIT) Frequency Cluster Data

The HYSPLIT model is a complete system that computes simple air parcel trajectories and complex transport, dispersion, chemical transformation, and deposition simulations using meteorological data [52,53]. It was developed by the National Oceanic and Atmospheric Administration (NOAA) Air Resources Laboratory (ARL) [52,54]. This model can track and forecast the release of dust, ash, volcanic ash and pollutants from various stationary and mobile emission sources [52]. The simulations were produced as trajectories, which could be clustered and presented by their mean trajectory. Trajectories were clustered using the similarity principle: data objects with higher similarity were grouped, while those with higher heterogeneity were separated into different groups [53]. The trajectories were combined until the total variance of the individual trajectories about their cluster mean started to increase substantially [54].

Version 5.2.0 of the HYSPLIT model was used to determine the trajectories of the air masses that arrived at Wakkerstroom during 2020 and 2021, possibly loaded with pollutants, affecting the NO₂ tropospheric levels. The backward trajectories were simulated at 700 hPa and 550 hPa. These levels were informed by the a priori profile shapes from the TROPOMI retrieved TVC-NO₂ concentrations and the atmospheric partial profiles of the Pandora-derived TVC-NO₂ concentrations from January 2020 to December 2021. The HYSPLIT model simulated and merged five-day backward trajectories to produce backward trajectory clusters for 2020 and 2021, respectively. The trajectories were merged

into 4 clusters according to their spatial variance. The resultant clusters were used to determine the nature and extent of primary air mass transport to Wakkerstroom. They distinguish between oceanic, clean continental, and polluted continental air mass transport. Transport pathways concerning synoptic circulation patterns assume that air masses mix as part of these circulation patterns [55].

This study used five-day backward trajectories instead of one- or two-day backward trajectories, even in light of the short lifetime of atmospheric NO₂. Five-day backward trajectories were used because South Africa's atmosphere is predominantly stable under the influence of the continental high-pressure system that prevails for most days of the year. Short timescale backward trajectories might not show the recirculation patterns or the source of the TVC-NO₂ concentrations.

3. Results

3.1. Tropospheric Vertical Column NO₂ Concentrations

This section reports the integrated tropospheric vertical column nitrogen dioxide concentrations observed by the Pandora-2s and the TROPOMI satellite instruments at Wakkerstroom, Mpumalanga, from January 2020 to December 2021.

3.1.1. Annual Concentrations

The annual mean and median NO₂ concentrations in the lower tropospheric vertical column (LTVC) (1780 m to 6730 m a.s.l.) retrieved using the MAX-DOAS Pandora technique are given in Table 2, together with the TROPOMI-derived TVC-NO₂ concentrations in Table 3.

Table 2. Interannual comparison of integrated MAX-DOAS tropospheric vertical column nitrogen dioxide mean and median diurnal concentrations measured by the ground-based Pandora at Wakkerstroom in 2020 and 2021.

| Year | Tropospheric Vertical Column NO ₂ (mol/m ²) | |
|-----------------|--|-----------------------|
| | Annual Mean (±Stdev) | Annual Median |
| 2020 | $5.06 \times 10^{-5} \pm 8.97 \times 10^{-5}$ | 2.10×10^{-5} |
| 2021 | $5.03 \times 10^{-5} \pm 9.40 \times 10^{-5}$ | 1.44×10^{-5} |
| <i>p</i> -value | >0.05 | <0.05 |

Table 3. The diurnal mean and median tropospheric vertical column nitrogen dioxide concentrations in 2020 and 2021 measured in Wakkerstroom using the TROPOMI satellite.

| Year | Tropospheric Vertical Column NO ₂ (mol/m ²) | |
|-----------------|--|-----------------------|
| | Annual Mean (±Stdev) | Annual Median |
| 2020 | $6.17 \times 10^{-5} \pm 1.06 \times 10^{-4}$ | 2.86×10^{-5} |
| 2021 | $7.06 \times 10^{-5} \pm 1.04 \times 10^{-4}$ | 2.94×10^{-5} |
| <i>p</i> -value | >0.05 | >0.05 |

The Pandora-derived concentrations at Wakkerstroom for 2020 ($5.06 \times 10^{-5} \pm 8.97 \times 10^{-5}$ mol/m²) were statistically similar (*p*-value > 0.05) to those in 2021 ($5.03 \times 10^{-5} \pm 9.40 \times 10^{-5}$ mol/m²) (Table 2). These values also align with the Ozone Monitoring Instrument (OMI)-derived results reported by Matandirotya and Burger [16] for 2019 and 2020 over Johannesburg. Johannesburg is adjacent to the Highveld area and the two air sheds are known to influence one another [56]. It also indicates that the values are, on average, representative of this hotspot of NO₂ emissions in South Africa.

Compared with other commercial and industrial regions around the world, the annual mean concentrations at Wakkerstroom in 2020 are similar to mean concentrations at sites in

midwestern Brazil in the same year measured using the OMI satellite instrument and not a ground-based instrument [57].

Due to the gamma distribution pattern of atmospheric NO₂ concentrations and other atmospheric variables, the median is a more reliable measure of central tendency. However, the median values measured at Wakkerstroom for the two years are not the same. The median concentrations in 2020 (2.10×10^{-5} mol/m²) are significantly higher (p -value < 0.05) than in 2021 (1.44×10^{-5} mol/m²) (Table 2).

The mean and median TROPOMI-derived annual TVC-NO₂ concentrations were $6.17 \times 10^{-5} \pm 1.06 \times 10^{-4}$ mol/m² and 2.86×10^{-5} mol/m², respectively, in 2020 (Table 3). They were not significantly different (p -value > 0.05) from the values measured during 2021 ($7.06 \times 10^{-5} \pm 1.04 \times 10^{-4}$ mol/m² and 2.94×10^{-5} mol/m²).

The annual mean and median TVC-NO₂ concentrations derived from TROPOMI are higher than the Pandora-derived TVC-NO₂ concentrations. This is expected since the Pandora instrument only accounts for approximately 1/3 of the tropospheric column compared to the total tropospheric column derived from the TROPOMI instrument. The similar interannual mean concentrations found in this study from both instruments suggest the dominance of regionally significant factors influencing tropospheric NO₂ levels, particularly in the low troposphere, over the Highveld.

The ground-based Pandora data at Wakkerstroom indicate that the emissions in the LTVC were significantly higher in 2020 than in 2021, but in the total tropospheric column data from the TROPOMI instrument, there were no significant changes.

The TVC-NO₂ concentrations at Wakkerstroom are highly variable, as shown by the large standard deviation around the mean concentrations of the highly temporally resolved data (Tables 2 and 3). The variation can be attributed to anthropogenic and natural factors such as changes in local emissions, atmospheric circulation and stability, air mass transport, and weather patterns [23,58].

To explore this variability, we analysed the seasonality of the data. In South Africa, the seasons are delineated as follows: summer (December to February, DJF), autumn (March to May, MAM), winter (June to August, JJA), and spring (September to November, SON). Spring is characterised by the onset of rainfall over the region, while summer is the wet season. Autumn and winter are dry over the Highveld [59,60].

An overall season pattern emerges out of the weekly average MAX-DOAS data over Wakkerstroom. The early summer and early spring (late winter) seasons recorded the highest mean concentrations of LTVC-NO₂ over Wakkerstroom for both years. The highest Pandora-derived LTVC-NO₂ concentrations in 2020 were observed in the summer during week 50 (mean: $1.68 \times 10^{-4} \pm 1.88 \times 10^{-4}$ mol/m²; median: 9.33×10^{-5} mol/m²) (Figure 3).

While Figure 3 (2020 data) shows peak LTVC-NO₂ concentrations in austral summer, Figure 4 for 2021 data shows contrasting patterns of peak seasonal LTVC-NO₂ concentrations (mean: $1.63 \times 10^{-4} \pm 8.67 \times 10^{-5}$ mol/m²; median: 1.36×10^{-4} mol/m²) in late winter (week 34). The lowest mean ($5.51 \times 10^{-6} \pm 3.18 \times 10^{-6}$ mol/m²) and median (4.83×10^{-6} mol/m²) LTVC-NO₂ concentrations were measured during the autumn and the early winter months, with the exception of one episode in week 23 (Table A1).

The TROPOMI data show a distinctly different seasonal pattern of highest and lowest concentrations of tropospheric NO₂. The observations from the satellite-based instrument show an early winter and early spring peak in both years. The lowest concentrations between 2020 and 2021 do not coincide. In 2020, the lowest concentrations are observed in late summer and early autumn (this is more or less the same as the ground-based data). In 2021, minimum concentrations are observed in the late summer period. The weekly aggregated TROPOMI-derived data show peak weekly mean TVC concentrations ($1.75 \times 10^{-4} \pm 3.71 \times 10^{-4}$ mol/m²) in the winter (in week 27) (Figure 5).

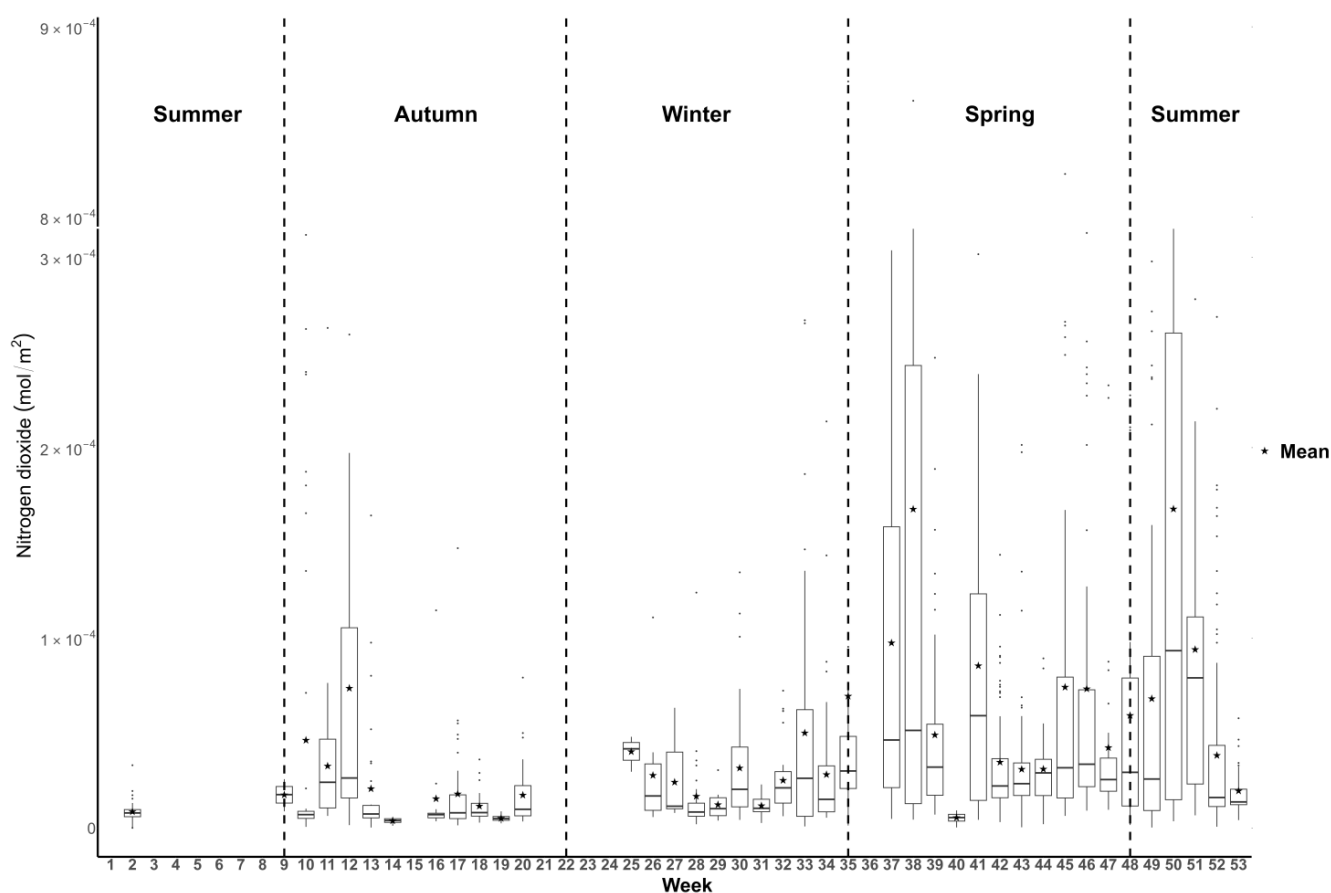


Figure 3. Boxplot of weekly averaged MAX-DOAS Pandora-derived low-tropospheric nitrogen dioxide concentrations (mol/m^2) in Wakkerstroom, Mpumalanga, for January to December 2020. A star denotes the weekly mean and the black dots represent all mean values higher than the upper quartile. The vertical dashed lines indicate the start of the four seasons: autumn, winter, spring and summer. The y-axis scale was cut between 3×10^{-4} and 8×10^{-4} mol/m^2 to make the figure more legible at low ($<3 \times 10^{-4}$ mol/m^2) NO_2 concentrations where the majority of the NO_2 concentrations measured. The data are expressed in full in Appendix B.

Further inspection of the TROPOMI-derived weekly data shows that during week 27, six out of the seven weekly measured concentrations were in the magnitude of $\times 10^{-5}$ except one, which was $\times 10^{-3}$. However, during week 39, only two of the six available daily concentrations were in the $\times 10^{-5}$ magnitude, and the rest were in the $\times 10^{-4}$. This indicates that a one-day event drove the high mean TVC- NO_2 concentration seen in week 27 (winter), while the elevated concentrations in spring were probably driven by the biomass-burning episodes during that week, as reported by [61].

The minimum mean ($3.33 \times 10^{-6} \pm 4.47 \times 10^{-6}$ mol/m^2) and median (2.47×10^{-6} mol/m^2) concentrations in 2020 were measured in week 13, autumn (Figure 5). This is due to the advection of clean air from the Southern Ocean observed at lower tropospheric levels during this time [61].

The 2021 TROPOMI-derived TVC- NO_2 data (Figure 6) show weekly mean ($3.16 \times 10^{-4} \pm 2.44 \times 10^{-4}$ mol/m^2) and median (2.68×10^{-4} mol/m^2) peaks in the late winter (week 34). The full data set can be seen in Appendix B. The similarity of this finding to that of the Pan159 LTVC- NO_2 concentrations (Figure 4) in the same year indicates that the low tropospheric sources contributed more to the integrated column concentrations.

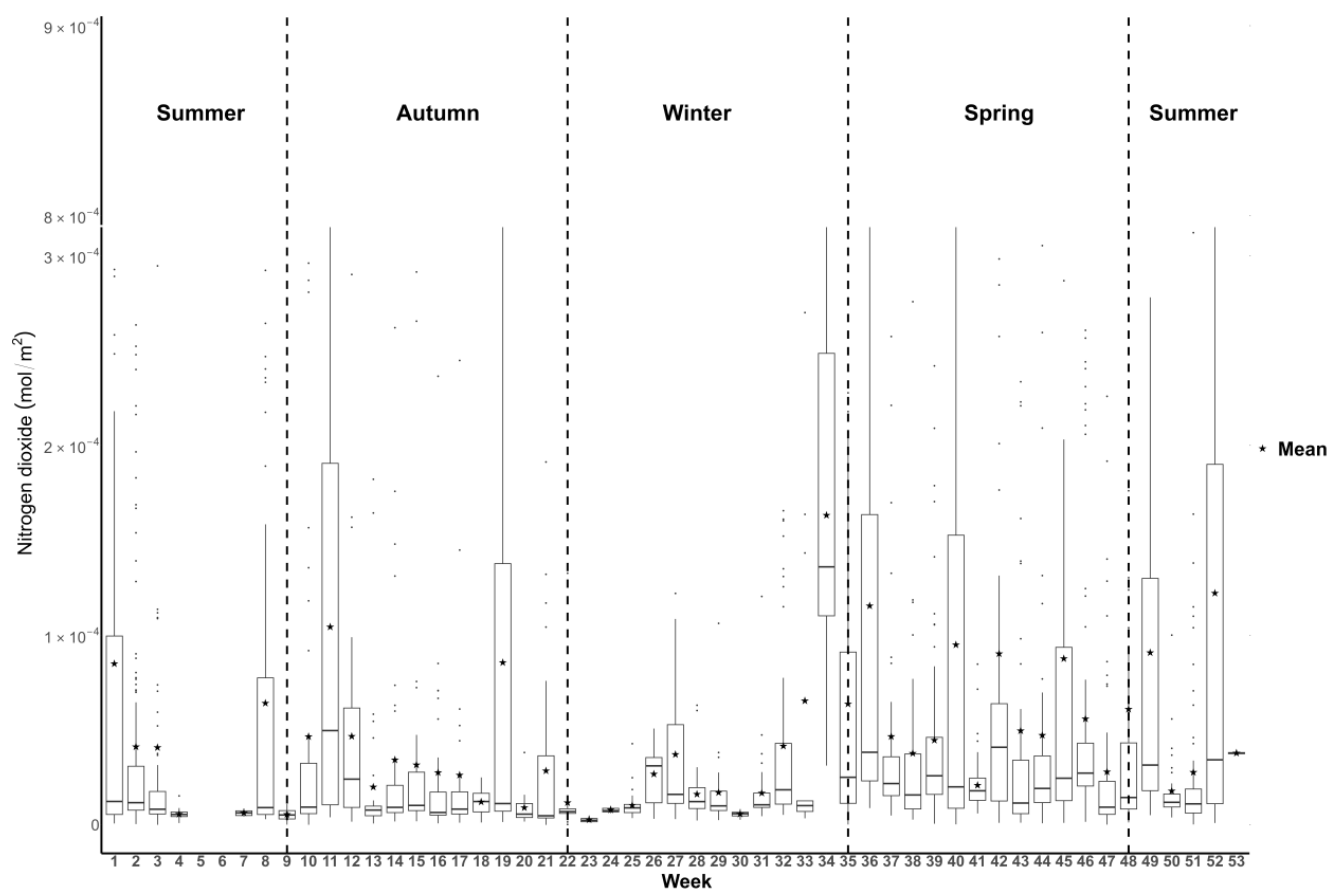


Figure 4. Weekly averaged boxplots of MAX-DOAS Pandora-derived low tropospheric nitrogen dioxide concentrations (mol/m^2) in Wakkerstroom, Mpumalanga, for 2021. A star denotes weekly means. The vertical dashed lines indicate the start of the four seasons: autumn, winter, spring and summer. The y-axis scale was cut between 3×10^{-4} and 8×10^{-4} mol/m^2 to make the figure more legible at low ($<3 \times 10^{-4}$ mol/m^2) NO_2 concentrations where the majority of the NO_2 concentrations measured. The data are expressed in full in Appendix B.

The elevated concentrations observed from the ground-based instrument were not the expected results. Although the concentrations in early summer 2021 are lower than in 2020, the concentrations remain higher than in winter. Previous studies have found elevated concentrations during the winter [56,62]. The difference is that the previous studies used ground-based in situ measurements that have no way of looking at the integrated tropospheric column. The elevated summer concentrations are surprising because this is the wet and warm season, associated with unstable meteorological conditions, increasing the vertical motion and dispersion of trace gases in the atmosphere [63,64]. In addition, the increased precipitation during the wet seasons increases the removal of pollutants from the atmosphere through wet deposition [17,56]. A key difference between the two seasons is the atmospheric stability, which determines the mixing of NO_2 from major sources through the column. It was expected that NO_2 measured in the tropospheric column would be integrated, thus not really showing a big difference between the seasons, especially summer and winter. It seems that the vertical mixing is impacting the detected concentrations. This is coupled with the transport pathways of NO_2 from the main source region, the industrialised Highveld, to the site. During summer, the transport pathway is controlled by the easterly wave perturbations [65].

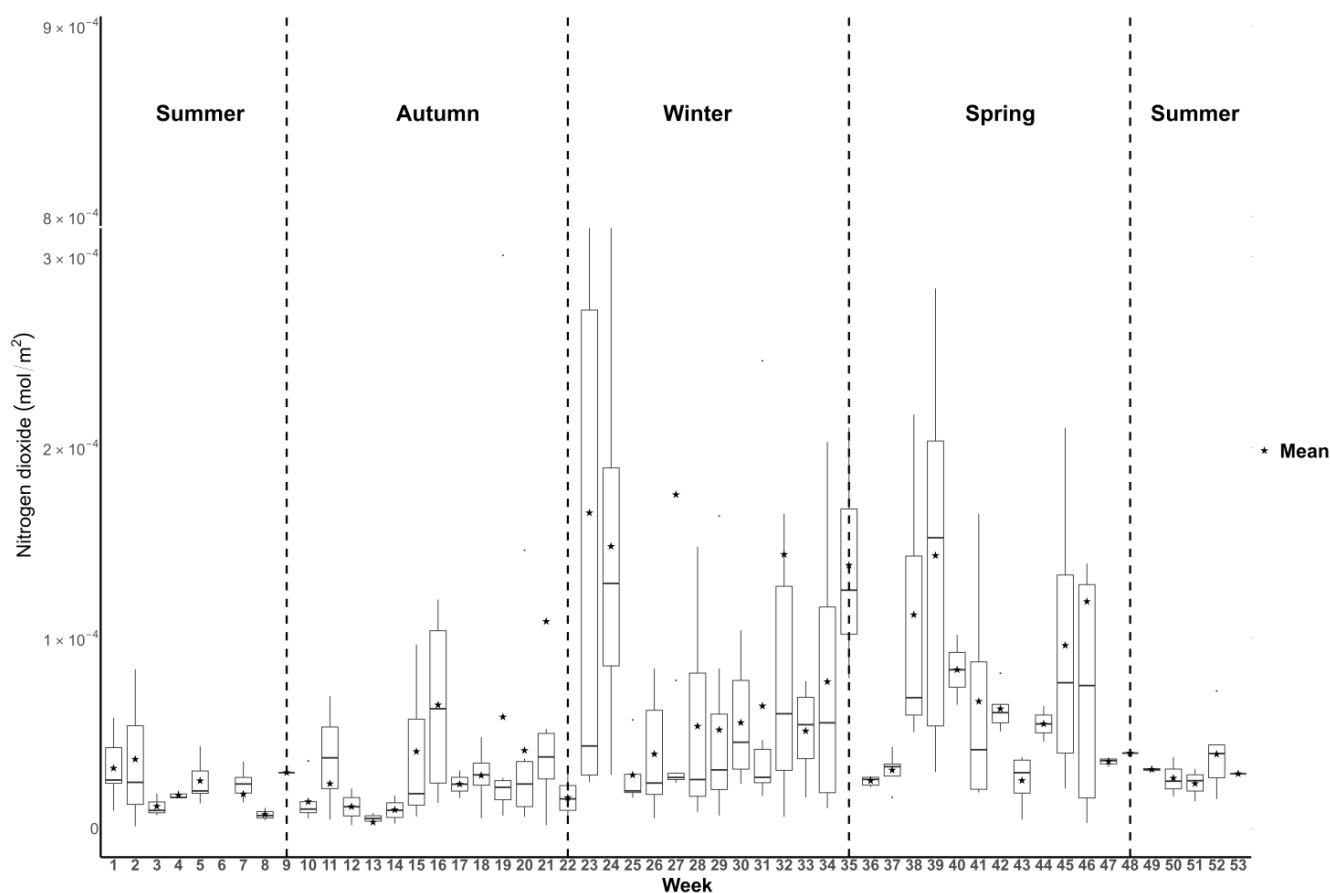


Figure 5. TROPOMI-derived tropospheric nitrogen dioxide concentrations over Wakkerstroom, Mpumalanga, averaged weekly for 2020. The means are represented by a star. The vertical dashed lines indicate the start of the four seasons: autumn, winter, spring and summer. The y-axis scale was cut between 3×10^{-4} and 8×10^{-4} mol/m² to make the figure more legible at low ($<3 \times 10^{-4}$ mol/m²) NO₂ concentrations where the majority of the NO₂ concentrations were measured. The data are expressed in full in Appendix B.

In contrast, winters are characterised by the formation of surface inversion layers inhibiting vertical atmospheric mixing and effectively trapping the primary pollutants [17]. The winters in the Highveld are dry and cold, resulting in additional combustion of coal and wood for domestic heating [17]. Furthermore, the transition from winter to spring and the spring are also characterised by occurrences of biomass burning [56].

These conflicting findings challenge the established understanding of TVC-NO₂ concentration patterns during the winter season.

Due to the lack of pollutant measurements in South Africa and the spatial and temporal variability, it would be extremely useful if the TROPOMI data could be utilised as a proxy of gaseous pollutant concentrations over the most polluted regions of South Africa. From the data presented in Figures 3–6, this seems not to be an ideal practice. On average (not considering the extreme values), however, if we compare the Pandora and TROPOMI tropospheric column data (Figure 7), we see that it is possible to use a longer-term average value (weekly) as a proxy of the state of gaseous pollutants over the Highveld. There are some differences, as one would expect, but overall, the TROPOMI data give a fair estimate of the NO₂ concentrations over Wakkerstroom, as they capture the majority of the integrated concentrations from the lower troposphere. The highest concentrations occur in the late winter and early spring, with early summer and winter also showing elevated levels of NO₂. The question that remains is whether Wakkerstroom is a representative site of the industrialised Highveld. Wakkerstroom is in close proximity to some of the

largest power plant emissions in South Africa. The site is also downwind of the industrial and urban complex of the Highveld. As with most sites over the Highveld, the site is also influenced by a series of other sources, namely local burning as well as the seasonal peak of biomass burning. We would argue that this analysis shows that TROPOMI can be used to generate proxies of indexes of air quality weekly or longer when longer-term average data are utilised.

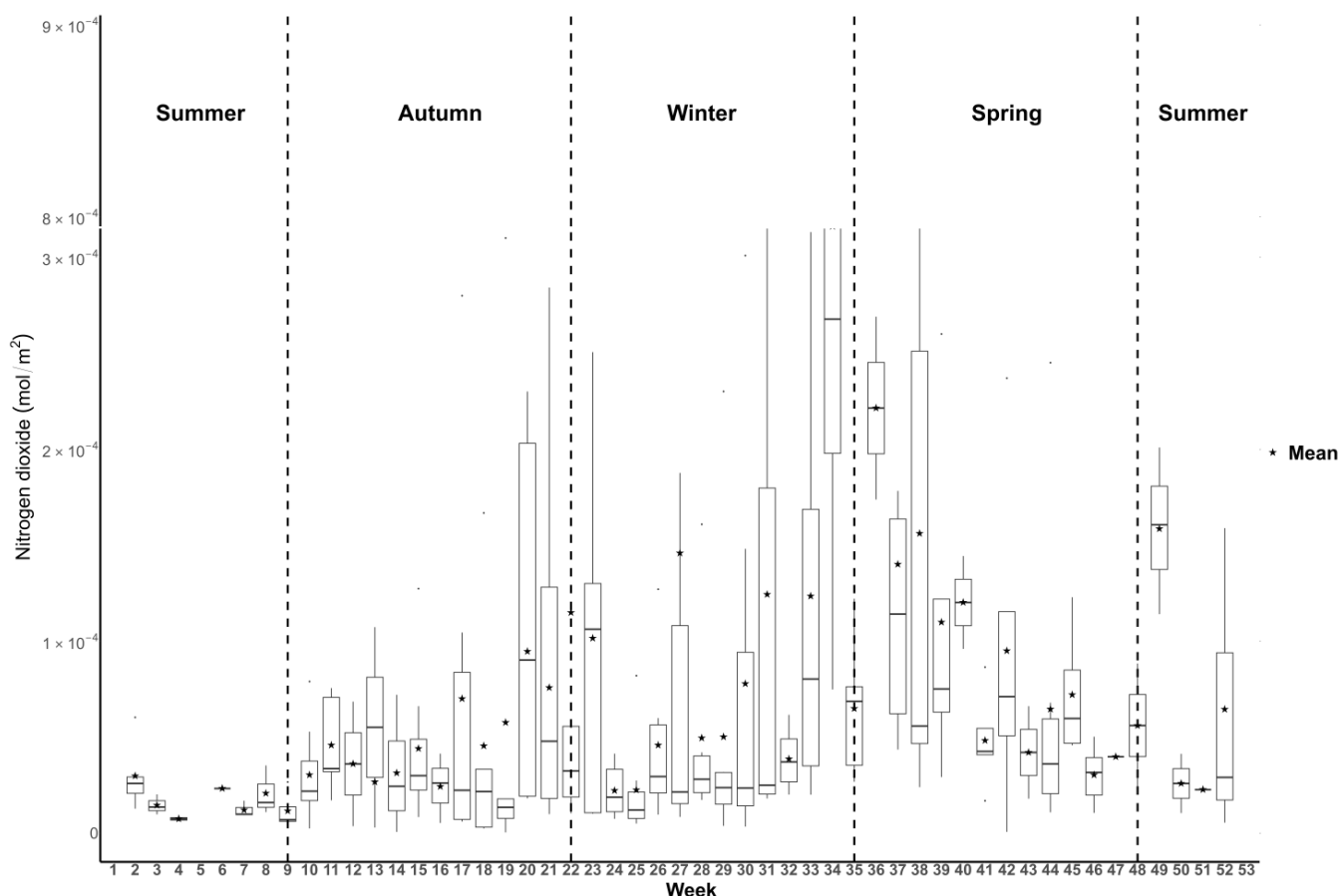


Figure 6. TROPOMI-derived tropospheric nitrogen dioxide concentrations over Wakkerstroom, Mpumalanga, averaged weekly for 2021. The means are represented by a star. The vertical line indicates the start of a new season. The vertical dashed lines indicate the start of the four seasons: autumn, winter, spring and summer. The y-axis scale was cut between 3×10^{-4} and 8×10^{-4} mol/m² to make the figure more legible at low ($<3 \times 10^{-4}$ mol/m²) NO₂ concentrations where the majority of the NO₂ concentrations were measured. The data are expressed in full in Appendix B.

For both instrument measurements, the mean TVC-NO₂ concentrations for 2020 and 2021 (Figure 7) at Wakkerstroom increased consistently during seasonal transitions, specifically from winter to spring. A more variable increase is seen in the transition between autumn and winter. Another consistency between the TROPOMI and Pandora TVC-NO₂ concentrations is the increase in concentrations in 2021 during the austral summer season (Figure 7). The high Pandora measurements reflect the local variability diurnally and temporally in the lower tropospheric column NO₂ concentrations. The TROPOMI data, in contrast, do not show that because of its daily overpass, unlike the Pan159 instrument that measures more frequently.

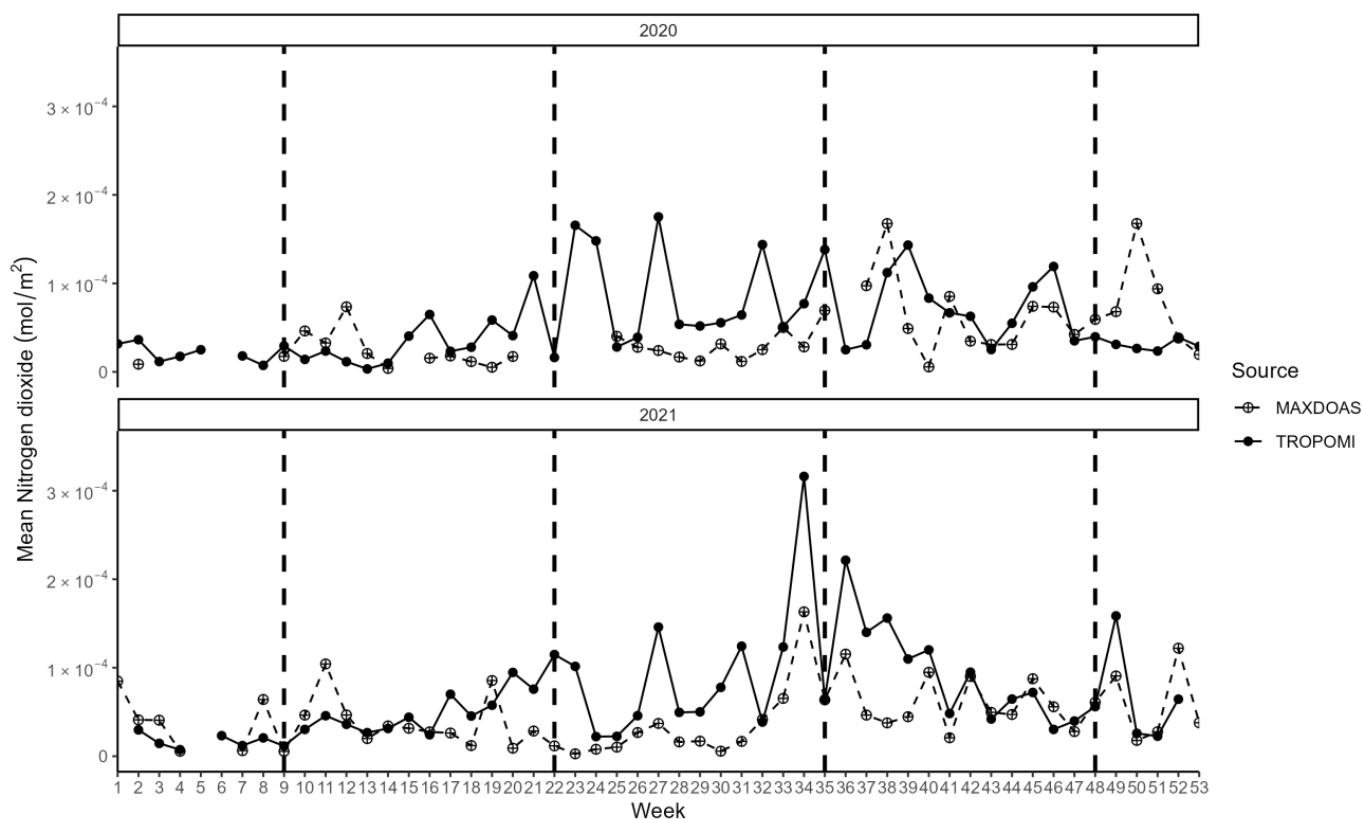


Figure 7. Comparison of weekly averaged TVC-NO₂ concentrations over Wakkerstroom, Mpumalanga, in 2020 (top panel) and 2021 (bottom panel), measured using TROPOMI (solid lines with solid circle) and Pandora instruments (MAX-DOAS) (dash lines with open circle).

3.1.2. TROPOMI and Pandora-Derived Tropospheric NO₂ Concentrations

The TROPOMI-derived annual mean and median TVC-NO₂ concentrations in 2020 and 2021 were higher than the Pandora-derived concentrations for the same years (Tables 2 and 3). This is expected since the two instruments are sensitive at different tropospheric levels and retrieved TVC-NO₂ concentrations from two different integrated TVC volumes. The data sets were evaluated to further elucidate the complementary relationship between the two instruments' TVC-NO₂ data products.

The Theil Sen Regression analyses were performed using ± 5 min (± 5 min) (Figure 8 left panel) and ± 1 h (± 1 h) (Figure 8 right panel) Pandora-derived coincidence data to the TROPOMI sensing time to compare the TROPOMI and Pandora-derived TVC-NO₂ concentrations over Wakkerstroom. The two coincidence data sets (Figure 8) show a positive correlation between the TROPOMI and Pandora-derived data sets (p -value < 0.05). The ± 5 min ($n = 48$) coincidence data show a strong determination coefficient (R^2) of 0.64 with a slope of 1.1. The correlation between the TROPOMI and Pandora ± 1 h coincidence data ($n = 149$) (Figure 8 right panel) is strong ($R^2 = 0.57$) but less than that of the ± 5 min data. There is a stronger correlation between the TROPOMI and the Pandora data sets when TVC-NO₂ concentrations are lower (Figure 8). This is probably because the majority of the concentrations measured are from the low troposphere where both instruments are measuring.

The RSE values were used to validate the regression models, and all models are valid with RSE values approaching zero.

Further analyses of the ± 1 h coincidence data show that concentrations in summer are better correlated than during other seasons (Figure 9).

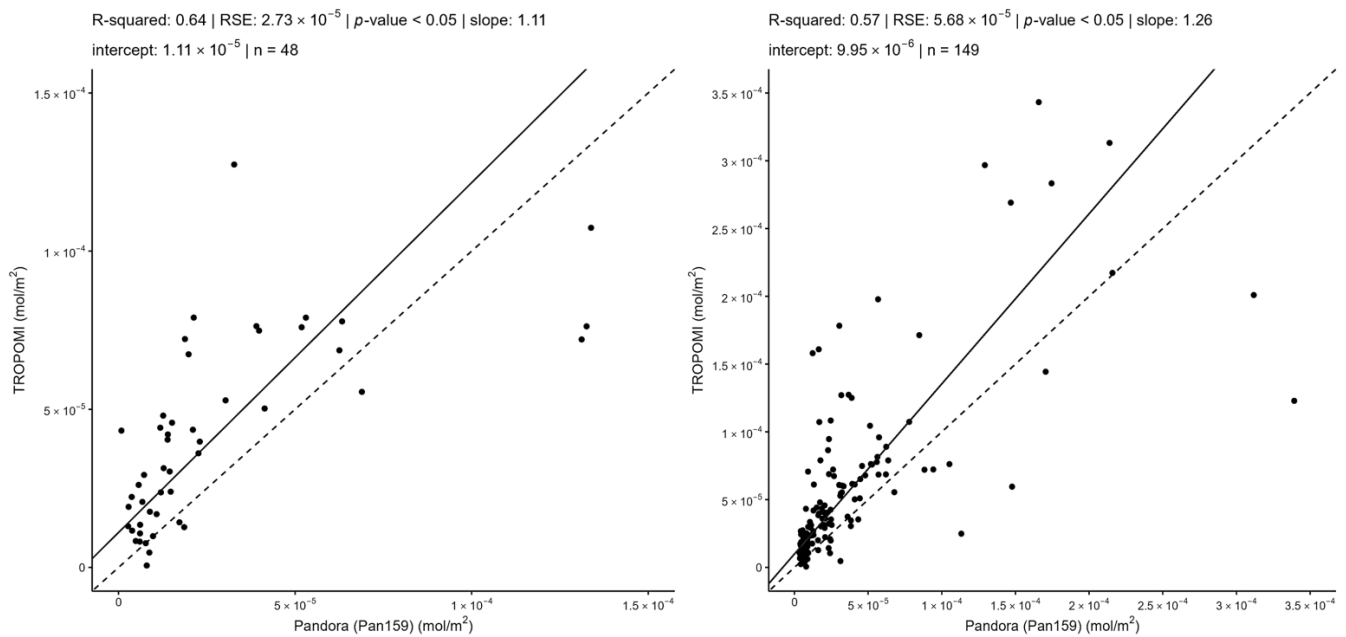


Figure 8. Theil Sen regression analysis of ± 5 min (left panel) and ± 1 h (right panel) coincidence TROPOMI and Pandora data over Wakkerstroom in 2020 and 2021. The black dashed line is the 1:1 line, and the black solid line is the regression line (± 5 min NMB%~54%; ± 1 h NMB%~64%).

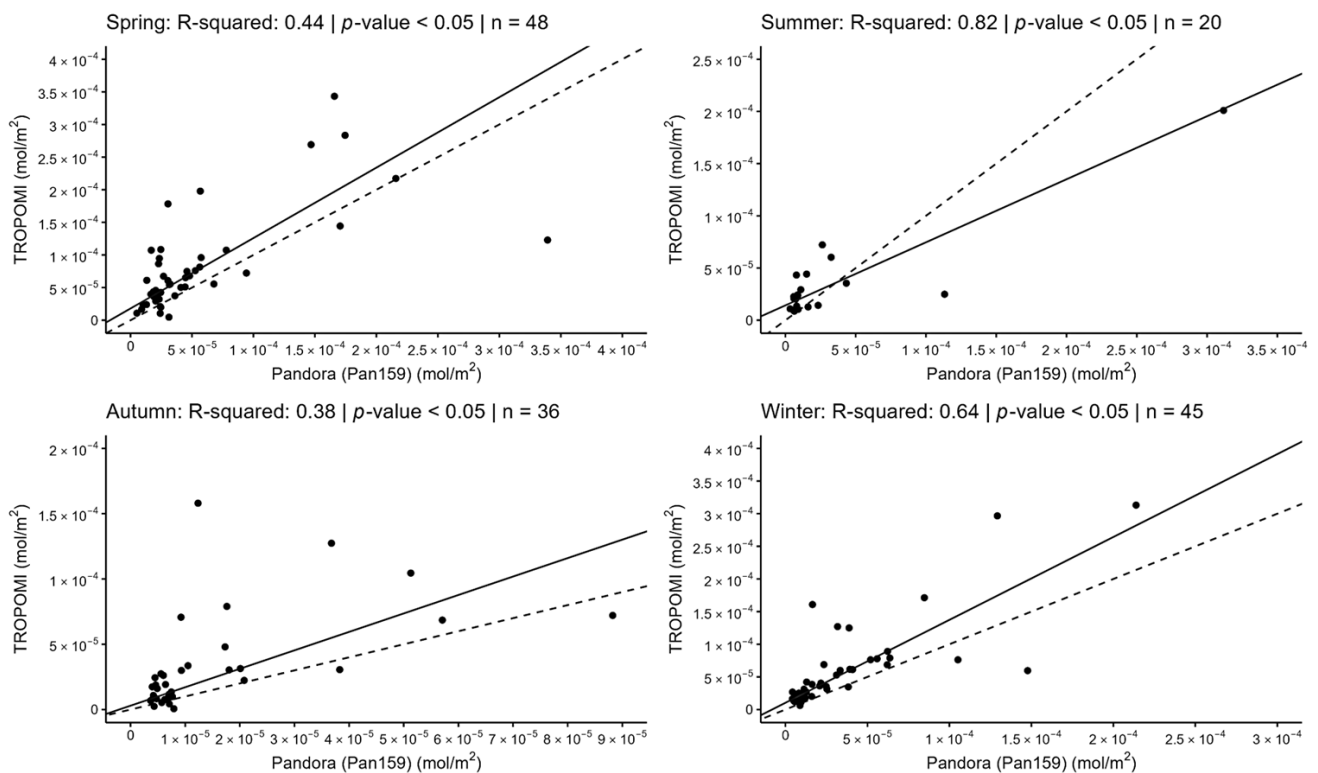


Figure 9. The seasonal correlation between the TROPOMI sensing time and the ± 1 h Pandora coincidence data over Wakkerstroom using the Theil Sen regression analysis. The black dashed line is the 1:1 line, and the black solid line is the regression line.

Diverse factors play a role in this disagreement between TROPOMI and Pan159 data sets, including averaging differences [2], different viewing geometries of the instruments, and NO_2 concentrations that are not uniformly mixed throughout the troposphere due

to emissions and vertical atmosphere mixing [66]. The Pandora-derived MAX-DOAS concentrations are predominantly in the lower troposphere, whereas the TROPOMI-derived concentrations are aggregated for the entire tropospheric column. The last of the factors explaining the disagreement in the TVC-NO₂ concentrations of the two instruments is especially important in the southern African context, where three dynamics exacerbate the problem of vertical stratification. Firstly, the interior of the South Africa Highveld is on an elevated plateau that is approximately 1700 m or more above sea level. Those elevations mean the major local emissions can be trapped closer to the ground due to temperature inversion [67,68]. In addition, the dispersion of pollutants on the Highveld may not be as efficient at lower elevations due to the low air density at higher elevations. Secondly, southern Africa has been shown to have a highly stratified vertical atmospheric structure that prevails for many months of the year. The atmospheric stratification is driven by subsidence, creating distinct and substantial thermodynamic barriers at approximately 3000 m and 5000 m a.s.l [69]. Finally, two major sources of NO₂ over the subcontinent include biomass burning, with ground emissions that can be carried up to the middle troposphere by turbulence, and power station emissions that have stacks designed to release emissions at a height above the stable layer to avoid downward mixing of the emissions in the presence of surface layer conversions. These factors create conditions, especially over the Highveld, of distinctly elevated plumes of concentrated pollution that can persist in the atmosphere for many days [70].

The inconsistency in the seasonal trends of atmospheric trace gas concentrations in the Highveld, particularly for short-lived pollutants such as NO₂, from satellite and ground-based instruments, indicates that the persistent stable layers in the Highveld atmosphere contribute to the complexity and disparity of the measurements.

3.2. Tropospheric Vertical Column Nitrogen Dioxide Profiles

Figure 10 shows the Pandora MAX-DOAS LTVC-NO₂ concentrations as a function of altitude in 2020 and 2021. It confirms that the Pan159 instrument measures LTVC-NO₂ concentrations aggregated from ~50 m to 4.5 km above the ground. Between the maximum vertical distance of 2.5 km and 3.5 km a.g.l is where the Pandora instrument measured the highest concentrations of NO₂ in the low troposphere. At altitudes above 4 km a.g.l and below ~1.5 km a.g.l, the concentrations were low (Figure 10). Some of the highest Pandora MAX-DOAS LTVC-NO₂ concentrations were measured at ~3 km a.g.l.

There are several stable layers in the Highveld atmosphere that could act as a vertical barrier [69], interfering with the mixing of the emitted NO₂ concentrations in the atmosphere. The boundary layer is at approximately 1300 m a.g.l (700 hPa), followed by the 500 hPa stable layer, which is at approximately 3800 m a.g.l. The 500 hPa stable layer coincides with the decrease in concentrations higher than 4 km a.g.l. If emissions are released above the boundary, there is less possibility of those emissions mixing down since the layer traps pollutants separating the emissions above and below the layer [69]. This is possibly why high concentrations are seen between the 700 hPa and 500 hPa stable layers.

The Tracer Model version 5, massively parallel version (TM5-MP) chemistry transport model a priori profile shape data of the TROPOMI-derived TVC-NO₂ retrievals over Wakkerstroom, Mpumalanga, in South Africa, are presented in Figure 11. These data show the a priori profile shapes for the stratospheric and the tropospheric vertical columns in 2020 and 2021. The highest concentrations were recorded in the lower atmosphere, between 800 and 600 hPa.

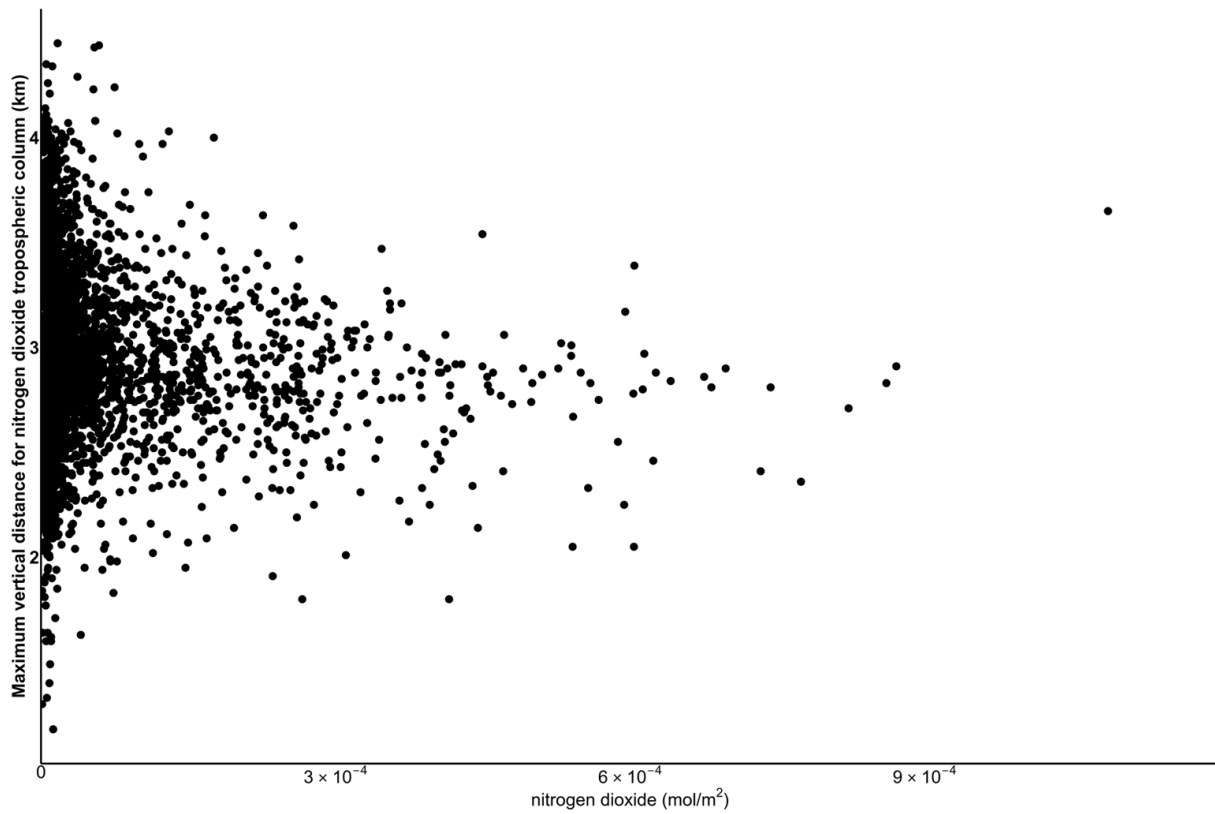


Figure 10. The maximum height Pandora MAX-DOAS tropospheric vertical column nitrogen dioxide profiles at Wakkerstroom, Mpumalanga Province. The vertical distance measured by Pan159 is above ground level (a.g.l). The altitude corresponds to atmospheric hPa (2 km a.g.l = ~650 hPa; 3 km a.g.l = ~550 hPa; 4 km a.g.l = ~500 hPa).

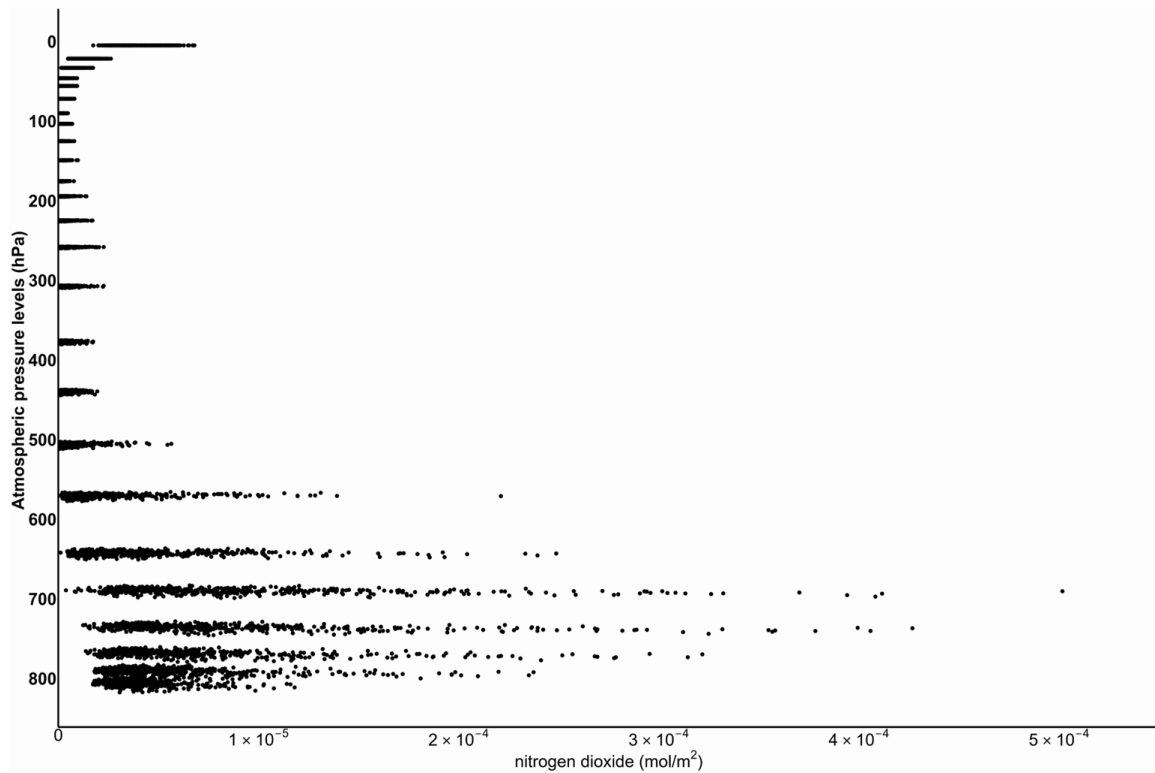


Figure 11. TROPOMI a priori profiles over the Wakkerstroom Highveld in 2020 and 2021.

3.3. Backward Trajectories (HYSPLIT)

In this research, three periods of elevated concentrations of NO_2 have been identified over Wakkerstroom. It is important to establish the atmospheric transport pathways associated with these increases in pollution to understand the potential contributing sources. Five-day backward trajectories have been used for this purpose.

In 2021, the late winter and early spring LTVC- NO_2 concentration peaks (week 34) were characterised by 50% air masses transported from the north of Wakkerstroom passing through the secondary hotspot over the Gauteng-Tshwane metro and coal-fired power station emissions at 550 hPa (Figure 12b). The air mass circulation was also dominated by continental recirculation patterns. The early summer LTVC- NO_2 concentration peaks in 2020 were associated with recirculation of air masses at the lower troposphere from Mozambique over Limpopo Province and the Johannesburg and Ekurhuleni urban Metros before reaching Wakkerstroom at an altitude of 3 km a.g.l. (Figure 12a). Additionally, 32% of the westerly air masses also pass over the Johannesburg-Tshwane metro and the clustered power stations over the MP Highveld before reaching Wakkerstroom at 550 hPa during early summer. These main trajectories (3 and 2) were approximately at or below the 550 hPa level.

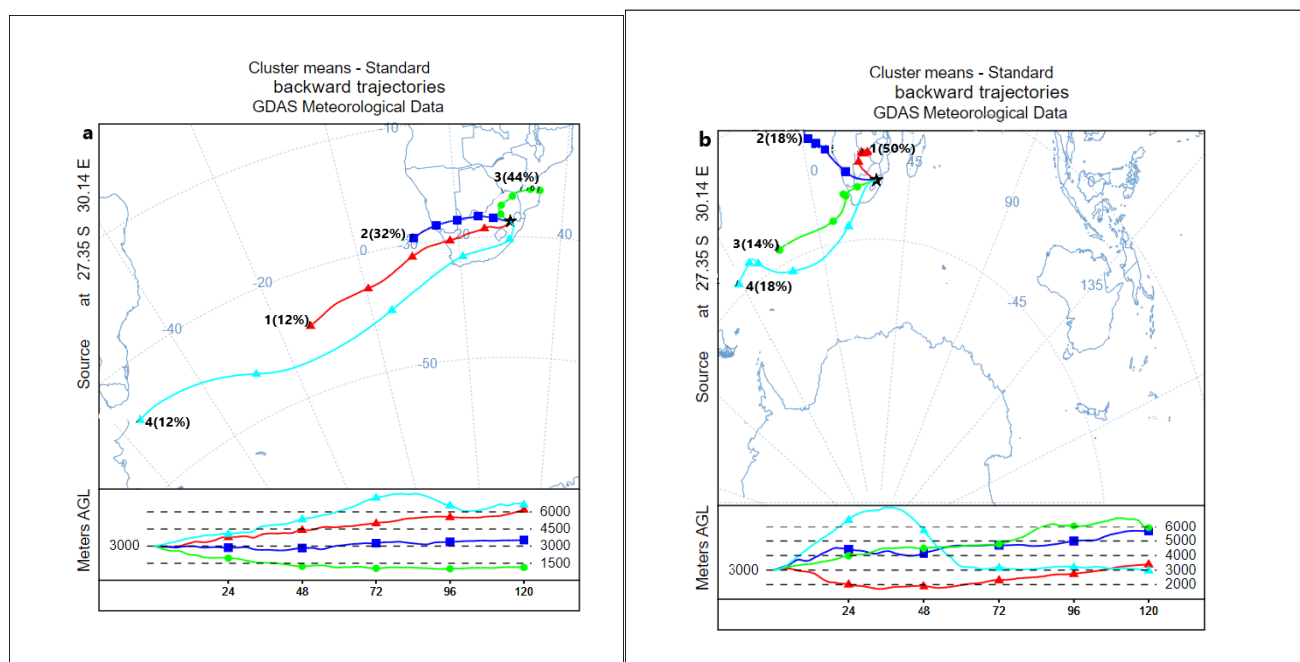


Figure 12. Five-day backward trajectories to Wakkerstroom, Mpumalanga, at 550 hPa for (a) week 50 in 2020 and (b) week 34 in 2021 for the observed peak LTVC- NO_2 concentrations measured by the Pan159 instrument.

These backward trajectories indicate sources of low-level emitters, such as biomass burning from southern Mozambique and local emissions from the Highveld. In addition, there are coal-fired power stations along that (from the west) transport pathway, causing additional loading of NO_2 concentrations as the air parcels are transported to Wakkerstroom. Fluctuations in local emissions are affected by shifts in commuting patterns of travellers passing through Volksrust from Johannesburg to KwaZulu-Natal or vice versa, the frequency of fossil fuel combustion and biomass burning. The literature has shown that fossil fuel combustion and biomass burning follow seasonal patterns, with increased fossil fuel combustion during the colder months (winter) and biomass burning from June to September in southern Africa [71,72].

The highest concentration of TVC- NO_2 identified from the TROPOMI satellite instrument was at ~ 700 hPa (Figure 11), which is more representative of the lower tropospheric

column. Therefore, backward trajectories at 700 hPa were investigated to find out what the major air mass trajectories were at that atmospheric level. In 2020, the transport patterns to Wakkerstroom were dominated by westerly and southwesterly winds (Figure 13a) from above 2500 m a.g.l. This was not surprising as westerly airflow increases significantly to the Highveld during the early winter season [23]. This type of transport is associated with air masses free of industrial emissions [23]. However, the trajectories in week 27 linger over land as they pass over the Gauteng-Tshwane metro and the clustered power stations before they reach Wakkerstroom, allowing for the accumulation of emissions. In 2021, the main transport (63%) was recirculated African flow (Figure 13b, cluster 1). This type of transport is prevalent at the 700 hPa level to the Highveld [23] in the early winter season. It promotes the accumulation of pollutants from neighbouring countries and areas around Wakkerstroom. This is an indication that most of the TROPOMI-derived TVC-NO₂ concentrations detected at Wakkerstroom in 2021 are due to emissions from elevated plumes caused by power stations, biomass burning, and other industries. These plumes easily reach the base of the 700 hPa stable layer.

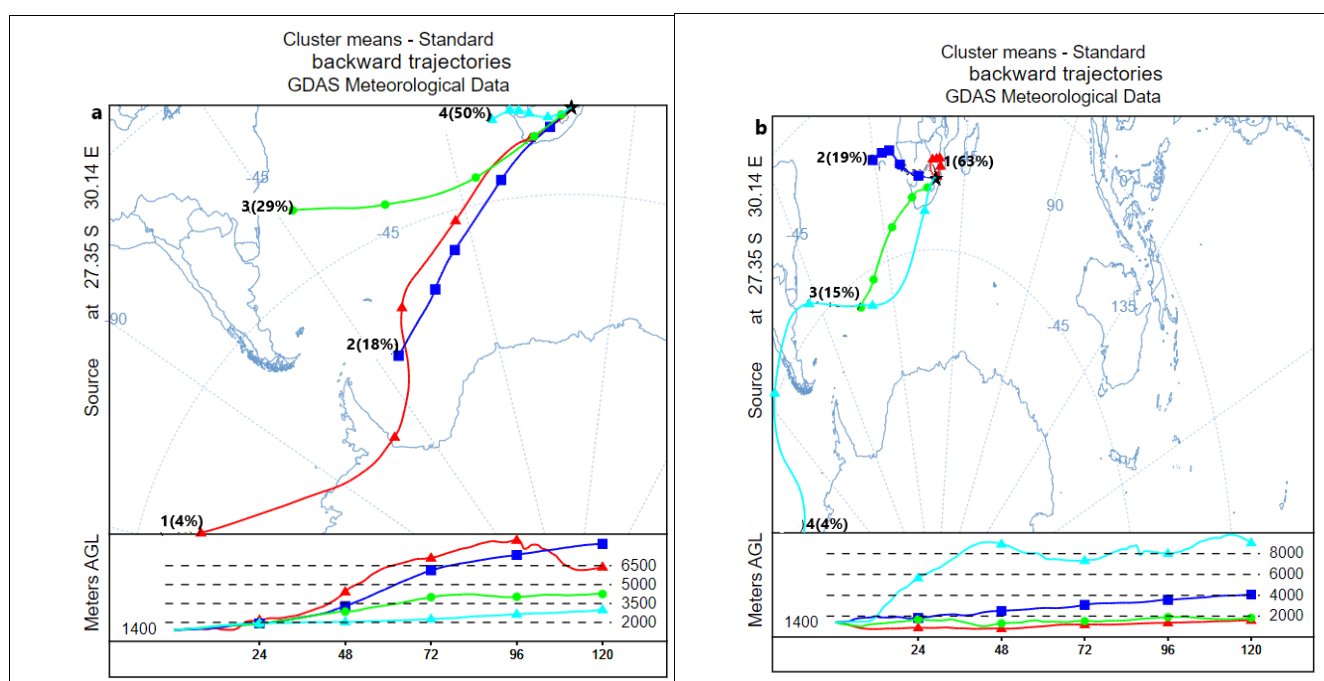


Figure 13. Five-day backward trajectories to Wakkerstroom, Mpumalanga, at 700 hPa for (a) week 27 in 2020 and (b) week 34 in 2021.

4. Discussion

The operation of the Pandora-2s instrument in the Mpumalanga Highveld of South Africa as part of the Pandonia Global Network (PGN) is significant as it is one of the only two Pandora instruments installed on continental Africa (https://blickm.pandonia-global-network.org/livemaps/pgn_stationsmap.png (accessed on 10 August 2024)), and it is located in an area subject to significant industrial pollution [56]. This is especially relevant because poor and deteriorating air quality is a major public health threat in this country. Furthermore, the high frequency of measurements available from the Pandora instrument effectively complement the wide spatial coverage but low frequency of data acquisitions from low earth orbiting (LEO) satellites, such as the TROPOMI satellite. Pandora-derived concentrations in this study are measured to an approximate maximum vertical atmospheric distance of 5 km above the ground (a.g.l). The highest concentration identifies the altitude of the highest concentrations of NO₂, as it was identified by the MAX-DOAS observations.

In contrast, the entire tropospheric column extends from the planetary surface (sea level or continental altitude) to 12 or 15 km.

The highest concentrations of tropospheric NO₂ are observed in the spring (late winter). Concentrations during this season are highly variable (Figures 3 and 4). The variability is likely associated with a source that is not fixed in space and variable in time. Biomass burning is the most likely source, as it is known to be transported over the Highveld during the spring season. From a previous analysis of lower tropospheric data derived from the Pandora instrument, it was shown that the emissions are transported towards the site from neighbouring South African countries—Mozambique and eSwatini—which contribute to the atmospheric NO₂ loading in the Highveld [61].

The reported elevated TVC-NO₂ concentrations can be attributed to the well-defined inversion layers that are present during winter, which trap pollutants, the slow wind speeds and recirculation patterns that limit dispersion as well as the absence of rainfall to scavenge the pollutants from the atmosphere [58,73,74]. In contrast, the 2020 median (1.52×10^{-4} mol/m²) peaked in spring (week 39). The spike in the TVC-NO₂ concentration median indicates an event that elevated the measured concentrations. This is similar to the elevated surface NO₂ concentrations reported in 2020 over Wakkerstroom, which resulted from biomass burning in eSwatini [61].

Biomass-burning emissions have been identified to represent a large perturbation to global atmospheric chemistry [75]. NO₂ concentrations peaking in September can be attributed to biomass-burning emissions from the east of Wakkerstroom and other sources from the surrounding low-cost townships. In addition, considering the location of the Pandora instrument—downstream from major NO₂ pollutant sources, but not located next to or within those sources—the changes in emissions from the surrounding power stations are also possible contributors to the observed NO₂ concentrations.

The use of Pandora MAX-DOAS measurements to compare the TROPOMI-derived TVC-NO₂ concentrations has shown that the Pandora MAX-DOAS technique increases the spatial and temporal compatibility of the two data sets. Implementing two or more azimuthal directions for sky-scan measurements will further close the gap of scarce, highly spatially and temporally resolved air quality data and complement the relatively high spatial resolution global data from the TROPOMI satellite.

The Pandora-derived MAX-DOAS concentration seasonal patterns changed from a seasonal high in the summer of 2020 to the winter of 2021, while the TROPOMI seasonal pattern showed high NO₂ concentrations in the winter of both years. The similarity in the 2021 peak winter TVC-NO₂ concentrations for both instruments (even though the TROPOMI instrument measured higher TVC-NO₂ concentrations) indicates the aligned spatial resolution between the two data sets attributed to the sky scan measurements at various elevation angles and the contribution of the regional low troposphere sources to the measured total TVC-NO₂ concentrations. The similar seasonal variations between the Pandora-derived LTVC-NO₂ concentrations and the TROPOMI-derived concentrations indicate that the sources in the lower troposphere contribute a larger portion to the tropospheric column than sources higher in the troposphere, such as transported NO₂-laden air masses. This is evident when interrogating the weekly averaged data instead of the annual data. Both instruments identified peak concentrations in the lower troposphere, showing that the TROPOMI instrument is a good proxy of NO₂ distribution over Wakkerstroom.

Recirculation, transport from southern Mozambique, and northern and westerly air-flow to Wakkerstroom were identified as the air mass transport pathways contributing significantly to the measured elevated LTVC- and TVC-NO₂ concentrations in Wakkerstroom.

The temporal heterogeneity of NO₂ over the Mpumalanga Highveld can be seen using the Pandora-2s and the TROPOMI satellite instruments. This study showed that MAX-DOAS measurements from Pandora correlate positively ($R > 0$) with the TROPOMI satellite data when using 5 min and 1 h contemporaneous data, respectively. Ascertaining the bias between TROPOMI and ground-based instrument measurements is more complex

for individual measurement stations. The overestimated TROPOMI measurements of the Pandora coincidence data are expected due to the sensitivity of the two instruments at different atmospheric levels during measurements. However, this shows that MAX-DOAS-derived TVC-NO₂ concentrations can represent the area of satellite-derived TVC-NO₂ concentrations even when measuring in one azimuthal direction; hence, similar mean seasonal patterns but different median-informed seasonal patterns.

This can be attributed to the spatiotemporal heterogeneity of NO₂ and the sensitivity of the instruments at different atmospheric levels and that of the satellite in highly polluted areas—reflection, absorption, refraction and scattering are increased throughout the column during high pollution events. The presence of aerosols and other pollutants in the atmosphere, particularly in the stable layers, causes the satellite instrument to be more sensitive to NO₂ at the high atmospheric layers where the MAX-DOAS-derived concentrations are not measured. This is caused by the path length of the light to the instrument in the presence of other pollutants, resulting in more light absorption by the NO₂ trace gas.

5. Conclusions

The Pandora-2s instrument data complement TROPOMI satellite data due to its high temporal resolution data. These complementary data sets have shown similar seasonal TVC NO₂ concentration peaks despite indicating a significant local lower troposphere source in the Wakkerstroom area. Power stations and other local sources, such as biomass burning, contribute to the observed NO₂ levels in the Highveld. Seasonal TVC-/LTVC-NO₂ spikes, particularly in winter, are linked to inversion layers, low wind speeds, recirculation, and a lack of rainfall, which trap pollutants. The elevated LTVC-NO₂ concentrations in the early spring are attributed to biomass burning in neighbouring regions like Mozambique and eSwatini. This source is transported to the Highveld and contributes to the atmospheric NO₂ load. The spatiotemporal heterogeneity of NO₂ and the sensitivity differences between MAX-DOAS (ground-based) and satellite instruments make it challenging to compare measurements directly. However, both can provide important data on NO₂ distribution in Wakkerstroom.

Author Contributions: Conceptualisation, R.F.K.-S., M.C.S., R.J.S., S.J.P. and R.M.G.; Methodology, R.F.K.-S., M.C.S., S.J.P., R.M.G. and R.J.S.; Formal Analysis, R.F.K.-S.; Investigation, R.F.K.-S.; Resources, R.F.K.-S.; Data Curation, R.F.K.-S., J.v.G. and H.H.; Writing—Original Draft Preparation, R.F.K.-S.; Writing—Review and Editing, R.F.K.-S., M.C.S., S.J.P., R.M.G., H.H. and J.v.G.; Visualization, R.F.K.-S.; Supervision, M.C.S., S.J.P. and R.M.G.; Project Administration, R.F.K.-S., M.C.S. and S.J.P.; Funding Acquisition, M.C.S., R.J.S. and S.J.P. All authors have read and agreed to the published version of the manuscript.

Funding: This research was funded by Prof. Mary C. Scholes, grant number MCH021, and Prof. Stuart J. Piketh through the Climatology Research Group (CRG) in the Unit for Environmental Science and Management at the North-West University.

Institutional Review Board Statement: Not applicable.

Informed Consent Statement: Not applicable.

Data Availability Statement: Publicly available datasets were analysed in this study. This data can be found here: <https://dataspace.copernicus.eu/> (accessed on 13 September 2023) for the TROPOMI data and http://data.pandonia-global-network.org/Wakkerstroom/Pandora159s1/L2/Pandora159s1_Wakkerstroom_L2_rnvs3p1-8.txt (accessed on 8 January 2023) for the Pandora-2s data.

Acknowledgments: We thank PI(s) and staff (local operator: Paul Grobler) for their effort in establishing and maintaining the Wakkerstroom Pandora (Pan159) instrument. The PGN is a bilateral project supported by funding from NASA and ESA. The authors would like to extend their sincere appreciation to Deborah Stein Zweers, Ankie Piters, Gaia Pinardi and Stephen Broccardo. A special thank you to Michel Verstraete and Stephen Broccardo for the discussion sessions. We also thank the Climate Research Group (CRG) from the North-West University in South Africa.

Conflicts of Interest: The authors declare no conflict of interest. The funders had no role in the design of the study; in the collection, analyses, or interpretation of data; in the writing of the manuscript; or in the decision to publish the results.

Appendix A

Table A1. Pandora MAX-DOAS retrieved weekly frequency (n) data capture in 2020 and 2021 over Wakkerstroom, South Africa.

| Week | n_2020 | n_2021 |
|------|--------|--------|
| 1 | 0 | 6 |
| 2 | 2 | 7 |
| 3 | 0 | 7 |
| 4 | 0 | 5 |
| 5 | 0 | 0 |
| 6 | 0 | 0 |
| 7 | 0 | 1 |
| 8 | 0 | 7 |
| 9 | 1 | 5 |
| 10 | 7 | 6 |
| 11 | 3 | 6 |
| 12 | 3 | 5 |
| 13 | 3 | 4 |
| 14 | 2 | 7 |
| 15 | 0 | 6 |
| 16 | 3 | 7 |
| 17 | 4 | 6 |
| 18 | 5 | 3 |
| 19 | 5 | 6 |
| 20 | 4 | 5 |
| 21 | 0 | 7 |
| 22 | 0 | 5 |
| 23 | 0 | 1 |
| 24 | 0 | 3 |
| 25 | 1 | 6 |
| 26 | 3 | 5 |
| 27 | 4 | 4 |
| 28 | 5 | 6 |
| 29 | 4 | 6 |
| 30 | 6 | 3 |
| 31 | 6 | 5 |
| 32 | 5 | 7 |
| 33 | 7 | 2 |

Table A1. Cont.

| Week | n_2020 | n_2021 |
|-------|--------|--------|
| 34 | 7 | 4 |
| 35 | 4 | 7 |
| 36 | 0 | 4 |
| 37 | 3 | 6 |
| 38 | 6 | 6 |
| 39 | 7 | 6 |
| 40 | 1 | 7 |
| 41 | 5 | 7 |
| 42 | 7 | 7 |
| 43 | 6 | 6 |
| 44 | 4 | 7 |
| 45 | 5 | 6 |
| 46 | 5 | 7 |
| 47 | 3 | 7 |
| 48 | 2 | 7 |
| 49 | 5 | 7 |
| 50 | 6 | 5 |
| 51 | 3 | 7 |
| 52 | 7 | 6 |
| 53 | 2 | 1 |
| Total | 171 | 279 |

Appendix B

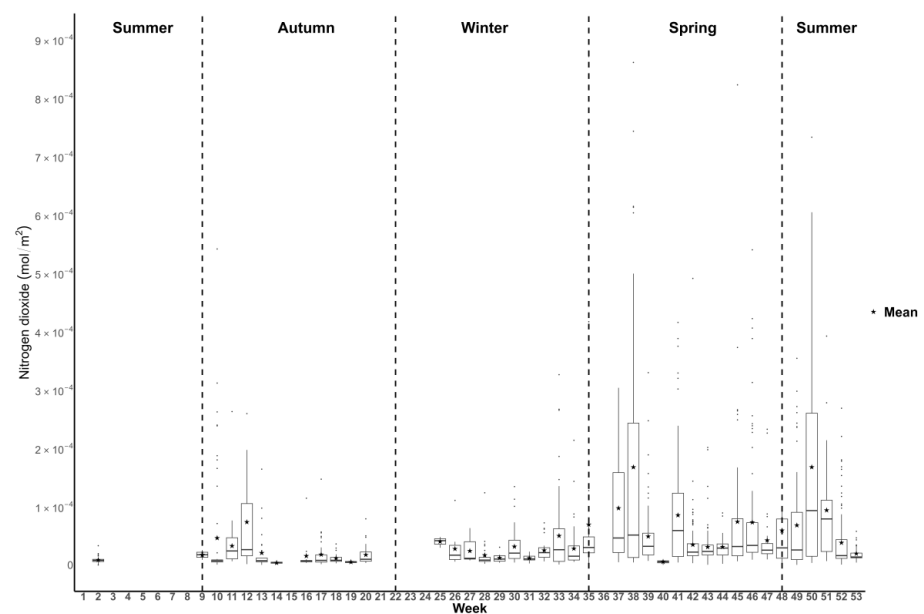


Figure A1. Boxplot of weekly averaged MAX-DOAS Pandora-derived low-tropospheric nitrogen dioxide concentrations (mol/m^2) in Wakkerstroom, Mpumalanga, for January to December 2020. A star denotes weekly means and the black dots represent all mean values higher than the upper

quartile. The vertical dashed lines indicate the start of the four seasons: autumn, winter, spring and summer. The y-axis scale was cut between 3×10^{-4} and 8×10^{-4} mol/m² to make the figure more legible at low ($<3 \times 10^{-4}$ mol/m²) NO₂ concentrations where the majority of the NO₂ concentrations were measured.

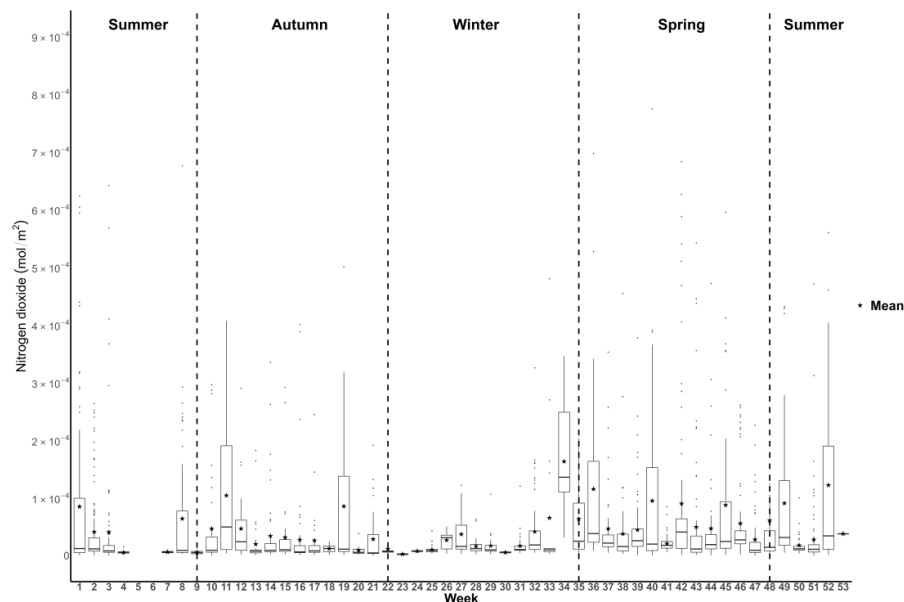


Figure A2. Weekly averaged boxplots of MAX-DOAS Pandora-derived low-tropospheric nitrogen dioxide concentrations (mol/m²) in Wakkerstroom, Mpumalanga, for 2021. A star denotes weekly means. The vertical dashed lines indicate the start of the four seasons: autumn, winter, spring and summer. The y-axis scale was cut between 3×10^{-4} and 8×10^{-4} mol/m² to make the figure more legible at low ($<3 \times 10^{-4}$ mol/m²) NO₂ concentrations where the majority of the NO₂ concentrations were measured.

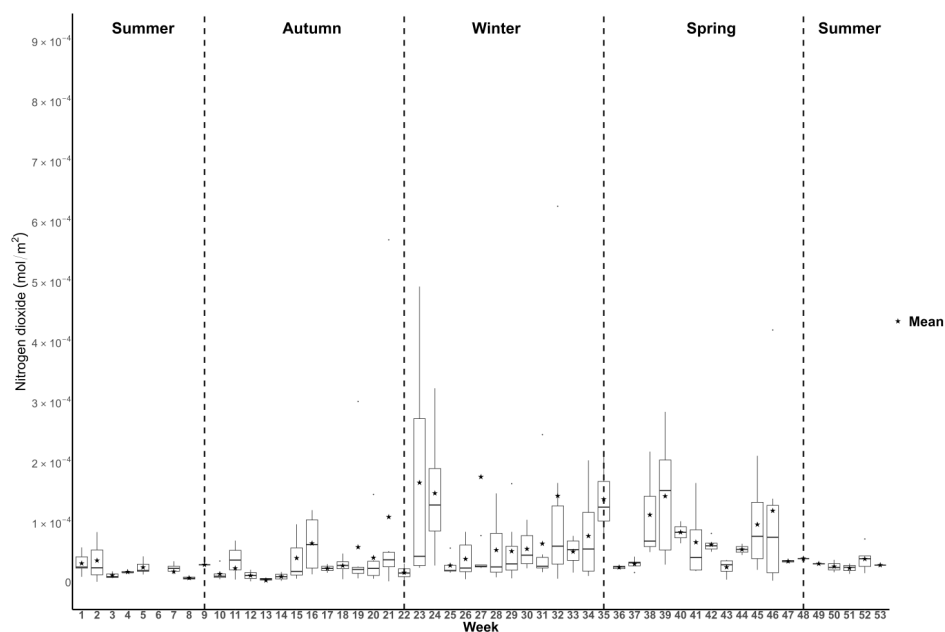


Figure A3. TROPOMI-derived tropospheric nitrogen dioxide concentrations over Wakkerstroom, Mpumalanga, averaged weekly for 2020. The means are represented by a star. The vertical dashed lines indicate the start of the four seasons: autumn, winter, spring and summer.

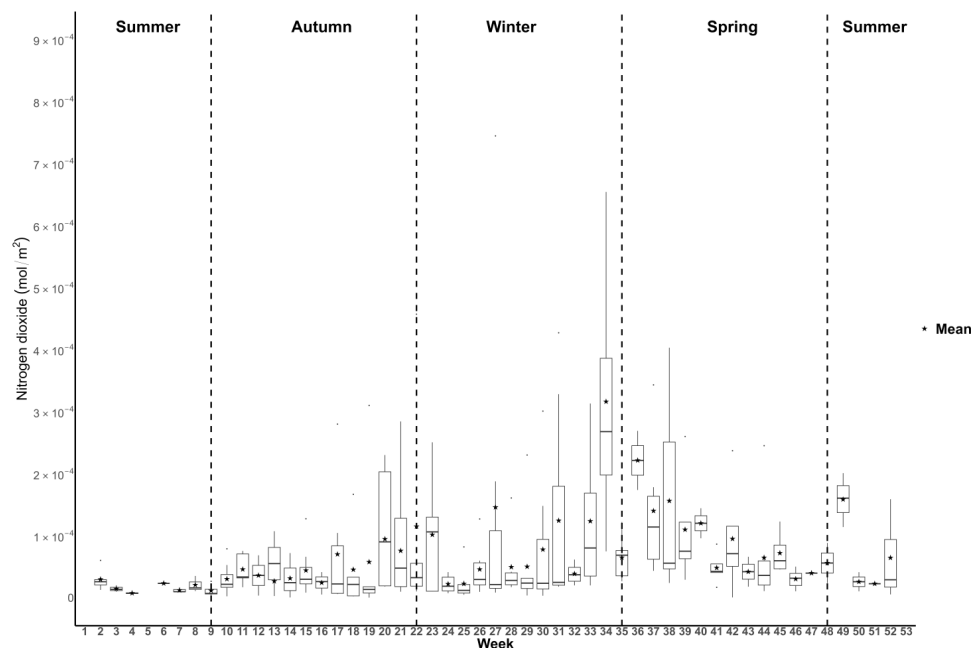


Figure A4. TROPOMI-derived tropospheric nitrogen dioxide concentrations over Wakkerstroom, Mpumalanga, averaged weekly for 2021. The means are represented by a star. The vertical line indicates the start of a new season. The vertical dashed lines indicate the start of the four seasons: autumn, winter, spring and summer.

References

- Judd, L.M.; Al-Saadi, J.A.; Szykman, J.J.; Valin, L.C.; Janz, S.J.; Kowalewski, M.G.; Eskes, H.J.; Veeckind, J.P.; Cede, A.; Mueller, M.; et al. Evaluating Sentinel-5P TROPOMI tropospheric NO₂ column densities with airborne and Pandora spectrometers near New York City and Long Island Sound. *Atmos. Meas. Tech.* **2020**, *13*, 6113–6140. [CrossRef] [PubMed]
- Benzerrouk, Z.; Abid, M.; Sekrafi, H. Pollution haven or halo effect? A comparative analysis of developing and developed countries. *Energy Rep.* **2021**, *7*, 4862–4871. [CrossRef]
- Tiseo, I. Nitrogen Oxide Emissions in the European Union 1990–2021, by Sector [WWW Document]. 2023. Available online: <https://www.statista.com/markets/408/energy-environment/> (accessed on 13 April 2024).
- Lourens, A.S.; Butler, T.M.; Beukes, J.P.; Van Zyl, P.G.; Beirle, S.; Wagner, T.K.; Heue, K.-P.; Pienaar, J.J.; Fourie, G.D.; Lawrence, M.G. Re-evaluating the NO₂ hotspot over the South African Highveld. *S. Afr. J. Sci.* **2012**, *108*, 6. [CrossRef]
- Vallero, D. Air Pollutant Hazards. In *Fundamentals of Air Pollution*, 5th ed.; Vallero, D., Ed.; Academic Press: Boston, MA, USA, 2014; Chapter 7; pp. 197–214. [CrossRef]
- Shikwambana, L.; Sivakumar, V. Investigation of various aerosols over different locations in South Africa using satellite, model simulations and LIDAR. *Meteorol. Appl.* **2019**, *26*, 275–287. [CrossRef]
- Shikwambana, L.; Mhangara, P.; Mbatha, N. Trend analysis and first time observations of sulphur dioxide and nitrogen dioxide in South Africa using TROPOMI/Sentinel-5 P data. *Int. J. Appl. Earth Obs. Geoinf.* **2020**, *91*, 102130. [CrossRef]
- Goldberg, D.L.; Lu, Z.; Streets, D.G.; De Foy, B.; Griffin, D.; Mclinden, C.A.; Lamsal, L.N.; Krotkov, N.A.; Eskes, H. Enhanced Capabilities of TROPOMI NO₂: Estimating NO_x from North American Cities and Power Plants. *Environ. Sci. Technol.* **2019**, *53*, 12594–12601. [CrossRef]
- Saxena, P.; Sonwani, S. *Criteria Air Pollutants and Their Impact on Environmental Health*; Springer Nature: Singapore, 2019. [CrossRef]
- Ashmore, M. Air Pollution. In *Encyclopedia of Biodiversity*, 2nd ed.; Levin, S.A., Ed.; Academic Press: Amsterdam, The Netherlands, 2013; pp. 136–147. [CrossRef]
- Fino, A. Air Quality Legislation. In *Encyclopedia of Environmental Health*, 2nd ed.; Nriagu, J., Ed.; Elsevier: Oxford, UK, 2019; pp. 61–70. [CrossRef]
- Gauss, M.; Ellingsen, K.; Isaksen, I.S.A.; Dentener, F.J.; Stevenson, D.S.; Amann, M.; Cofala, J. Changes in nitrogen dioxide and ozone over Southeast and East Asia between year 2000 and 2030 with fixed meteorology. *Terr. Atmos. Ocean. Sci.* **2007**, *18*, 475–492. [CrossRef]
- Adesina, J.A.; Piketh, S.J.; Qhekwana, M.; Burger, R.; Language, B.; Mkhathshwa, G. Contrasting indoor and ambient particulate matter concentrations and thermal comfort in coal and non-coal burning households at South Africa Highveld. *Sci. Total Environ.* **2020**, *699*, 134403. [CrossRef] [PubMed]
- Belelie, M.D.; Burger, R.P.; Mkhathshwa, G.; Piketh, S.J. Assessing the impact of Eskom power plant emissions on ambient air quality over KwaZamokuhle. *Clean Air J.* **2019**, *29*, 29–37. [CrossRef]

15. Beirle, S.; Platt, U.; Wenig, M.; Wagner, T. Highly resolved global distribution of tropospheric NO₂ using GOME narrow swath mode data. *Atmos. Chem. Phys.* **2004**, *4*, 1913–1924. [[CrossRef](#)]
16. Matandirotya, N.R.; Burger, R. An assessment of NO₂ atmospheric air pollution over three cities in South Africa during 2020 COVID-19 pandemic. *Air Qual. Atmos. Health* **2022**, *16*, 263–276. [[CrossRef](#)] [[PubMed](#)]
17. Laakso, L.; Vakkari, V.; Virkkula, A.; Laakso, H.; Backman, J.; Kulmala, M.; Beukes, J.P.; van Zyl, P.G.; Tiitta, P.; Josipovic, M.; et al. South African EUCAARI measurements: Seasonal variation of trace gases and aerosol optical properties. *Atmos. Chem. Phys.* **2012**, *12*, 1847–1864. [[CrossRef](#)]
18. Department of Forestry, Fisheries and the Environment. *National GHG Inventory Report South Africa: 2000–2020*; Department of Forestry, Fisheries and the Environment: Pretoria, South Africa, 2022.
19. Swap, R.J.; Annegarn, H.J.; Suttles, J.T.; King, M.D.; Platnick, S.; Privette, J.L.; Scholes, R.J. Africa burning: A thematic analysis of the Southern African Regional Science Initiative (SAFARI 2000). *J. Geophys. Res. Atmos.* **2003**, *108*, 8465. [[CrossRef](#)]
20. Medupi Power Station—Final Scoping Report [WWW Document]. 2005. Available online: https://www.eskom.co.za/OurCompany/SustainableDevelopment/EnvironmentalImpactAssessments/Pages/Medupi_Final_Scoping_Report.aspx (accessed on 12 April 2024).
21. Sillman, S. Tropospheric Ozone and Photochemical Smog. In *Treatise on Geochemistry*; Holland, H.D., Turekian, K.K., Eds.; Pergamon: Oxford, UK, 2003; pp. 407–431. [[CrossRef](#)]
22. Speight, J.G. Chemicals and the Environment. In *Environmental Organic Chemistry for Engineers*; Speight, J.G., Ed.; Butterworth-Heinemann: Oxford, UK, 2017; Chapter 1; pp. 1–41. [[CrossRef](#)]
23. Freiman, M.T.; Piketh, S.J. Air Transport into and out of the Industrial Highveld Region of South Africa. *J. Appl. Meteorol. Climatol.* **2003**, *42*, 994–1002. [[CrossRef](#)]
24. Rahal, F. Low-cost sensors, an interesting alternative for air quality monitoring in Africa. *Clean Air J.* **2020**, *30*, 1–2. [[CrossRef](#)]
25. Mbandi, A. Air Pollution in Africa in the time of COVID-19: The air we breathe indoors and outdoors. *Clean Air J.* **2020**, *30*, 1–3. [[CrossRef](#)]
26. Vandaele, A.C.; Hermans, C.; Simon, P.C.; Carleer, M.; Colin, R.; Fally, S.; Mérienne, M.F.; Jenouvrier, A.; Coquart, B. Measurements of the NO₂ absorption cross-section from 42,000 cm⁻¹ to 10,000 cm⁻¹ (238–1000 nm) at 220 K and 294 K. *J. Quant. Spectrosc. Radiat. Transf.* **1998**, *59*, 171–184. [[CrossRef](#)]
27. Finch, D.P.; Palmer, P.I.; Zhang, T. Automated detection of atmospheric NO₂ plumes from satellite data: A tool to help infer anthropogenic combustion emissions. *Atmos. Meas. Tech.* **2022**, *15*, 721–733. [[CrossRef](#)]
28. Douros, J.; Eskes, H.; van Geffen, J.; Boersma, K.F.; Compernelle, S.; Pinardi, G.; Blechschmidt, A.-M.; Peuch, V.-H.; Colette, A.; Veeffkind, P. Comparing Sentinel-5P TROPOMI NO₂ column observations with the CAMS regional air quality ensemble. *Geosci. Model Dev.* **2023**, *16*, 509–534. [[CrossRef](#)]
29. Verhoelst, T.; Compernelle, S.; Pinardi, G.; Lambert, J.-C.; Eskes, H.J.; Eichmann, K.-U.; Fjæraa, A.M.; Granville, J.; Niemeijer, S.; Cede, A.; et al. Ground-based validation of the Copernicus Sentinel-5P TROPOMI NO₂ measurements with the NDACC ZSL-DOAS, MAX-DOAS and Pandonia global networks. *Atmos. Meas. Tech.* **2021**, *14*, 481–510. [[CrossRef](#)]
30. Xue, R.; Wang, S.; Zhang, S.; He, S.; Liu, J.; Tanvir, A.; Zhou, B. Estimating city NO_x emissions from TROPOMI high spatial resolution observations—A case study on Yangtze River Delta, China. *Urban Clim.* **2022**, *43*, 101150. [[CrossRef](#)]
31. van Geffen, J.; Eskes, H.; Compernelle, S.; Pinardi, G.; Verhoelst, T.; Lambert, J.-C.; Sneep, M.; ter Linden, M.; Ludewig, A.; Boersma, K.F.; et al. Sentinel-5P TROPOMI NO₂ retrieval: Impact of version v2.2 improvements and comparisons with OMI and ground-based data. *Atmos. Meas. Tech.* **2022**, *15*, 2037–2060. [[CrossRef](#)]
32. Lorente, A.; Boersma, K.F.; Yu, H.; Dörner, S.; Hilboll, A.; Richter, A.; Liu, M.; Lamsal, L.N.; Barkley, M.; De Smedt, I.; et al. Structural uncertainty in air mass factor calculation for NO₂ and HCHO satellite retrievals. *Atmos. Meas. Tech.* **2017**, *10*, 759–782. [[CrossRef](#)]
33. Cooper, M.; Martin, R.; Henze, D.; Jones, D. Effects of a priori profile shape assumptions on comparisons between satellite NO₂ columns and model simulations. *Atmos. Chem. Phys.* **2020**, *20*, 7231–7241. [[CrossRef](#)]
34. Ialongo, I.; Virta, H.; Eskes, H.; Hovila, J.; Douros, J. Comparison of TROPOMI/Sentinel-5 Precursor NO₂ observations with ground-based measurements in Helsinki. *Atmos. Meas. Tech.* **2020**, *13*, 205–218. [[CrossRef](#)]
35. Hönninger, G.; von Friedeburg, C.; Platt, U. Multi axis differential optical absorption spectroscopy (MAX-DOAS). *Atmos. Chem. Phys.* **2004**, *4*, 231–254. [[CrossRef](#)]
36. Choi, S.; Lamsal, L.N.; Follette-Cook, M.; Joiner, J.; Krotkov, N.A.; Swartz, W.H.; Pickering, K.E.; Loughner, C.P.; Appel, W.; Pfister, G.; et al. Assessment of NO₂ observations during DISCOVER-AQ and KORUS-AQ field campaigns. *Atmos. Meas. Tech.* **2020**, *13*, 2523–2546. [[CrossRef](#)]
37. Prunet, P.; Lezeaux, O.; Camy-Peyret, C.; Thevenon, H. Analysis of the NO₂ tropospheric product from S5P TROPOMI for monitoring pollution at city scale. *City Environ. Interact.* **2020**, *8*, 100051. [[CrossRef](#)]
38. Cede, A.; Tiefengraber, M.; Gebetsberger, M.; Spinei Lind, E. Pandonia Global Network Data Products Readme Document, V1.8-3, Tech. rep. 2021. Available online: https://www.pandonia-global-network.org/wp-content/uploads/2021/01/PGN_DataProducts_Readme_v1-8-3.pdf. (accessed on 10 October 2022).
39. Dimitropoulou, E.; Hendrick, F.; Pinardi, G.; Friedrich, M.M.; Merlaud, A.; Tack, F.; De Longueville, H.; Fayt, C.; Hermans, C.; Laffineur, Q.; et al. Validation of TROPOMI tropospheric NO₂ columns using dual-scan multi-axis differential optical absorption spectroscopy (MAX-DOAS) measurements in Uccle, Brussels. *Atmos. Meas. Tech.* **2020**, *13*, 5165–5191. [[CrossRef](#)]

40. Lynch, J.; Cain, M.; Frame, D.; Pierrehumbert, R. Agriculture's Contribution to Climate Change and Role in Mitigation Is Distinct from Predominantly Fossil CO₂-Emitting Sectors. *Front. Sustain. Food Syst.* **2021**, *4*, 518039. [CrossRef]
41. Herman, J.; Cede, A.; Spinei, E.; Mount, G.; Tzortziou, M.; Abuhassan, N. NO₂ column amounts from ground-based Pandora and MFDOAS spectrometers using the direct-sun DOAS technique: Intercomparisons and application to OMI validation. *J. Geophys. Res. Atmos.* **2009**, *114*. [CrossRef]
42. Abad, G.G.; Souri, A.H.; Bak, J.; Chance, K.; Flynn, L.E.; Krotkov, N.A.; Lamsal, L.; Li, C.; Liu, X.; Miller, C.C.; et al. Five decades observing Earth's atmospheric trace gases using ultraviolet and visible backscatter solar radiation from space. *J. Quant. Spectrosc. Radiat. Transf.* **2019**, *238*, 106478. [CrossRef]
43. Cede, A.; Tiefengraber, M.; Gebetsberger, M.; Spinei Lind, E. Pandonia Global Network Data Products ReadmeDocument, V1.8-5, Tech. rep. 2022. Available online: https://www.pandonia-global-network.org/wp-content/uploads/2022/12/PGN_DataProducts_Readme_v1-8-6.pdf (accessed on 25 June 2023).
44. Pinardi, G.; Hendrick, F.; Clemer, K.; Lambert, J.-C.; Bai, J.; Roozendael, M.V. On the use of the maxdoas technique for the validation of tropospheric NO₂ column measurements from satellite. In Proceedings of the 2008 EUMETSAT Meteorological Satellite Conference, Darmstadt, Germany, 8–12 September 2008.
45. Cede, A.; Tiefengraber, M.; Gebetsberger, M.; Spinei Lind, E. Pandonia Global Network Data Products ReadmeDocument, V1.8-5, Tech. rep. 2021. Available online: https://www.pandonia-global-network.org/wp-content/uploads/2022/01/PGN_DataProducts_Readme_v1-8-5.pdf (accessed on 18 May 2023).
46. Azad, S.; Ghandehari, M. Emissions of nitrogen dioxide in the northeast U.S. during the 2020 COVID-19 lockdown. *J. Environ. Manag.* **2022**, *312*, 114902. [CrossRef]
47. Veefkind, J.P.; Aben, I.; McMullan, K.; Förster, H.; de Vries, J.; Otter, G.; Claas, J.; Eskes, H.J.; de Haan, J.F.; Kleipool, Q.; et al. TROPOMI on the ESA Sentinel-5 Precursor: A GMES mission for global observations of the atmospheric composition for climate, air quality and ozone layer applications. *Remote Sens. Environ.* **2012**, *120*, 70–83. [CrossRef]
48. Eskes, H.J.; van Geffen, J.H.G.M.; Boersma, K.F.; Eichmann, K.-U.; Pedernana, M.; Sneep, M.; Veefkind, J.P.; Loyola, D. *S5P/TROPOMI Level-2 Product User Manual Nitrogen Dioxide*; ESA: Paris, France, 2020.
49. Eskes, H.J.; Eichmann, K.-U. S5P MPC Product Readme Nitrogen Dioxide, Report S5P-MPC-KNMI-PRF-NO₂, V2.0, ESA. 2021. Available online: <https://sentinels.copernicus.eu/documents/247904/3541451/Sentinel-5P-NitrogenDioxide-Level-2-Product-Readme-File> (accessed on 23 September 2024).
50. Zhao, X.; Griffin, D.; Fioletov, V.; McLinden, C.; Cede, A.; Tiefengraber, M.; Müller, M.; Bogner, K.; Strong, K.; Boersma, F.; et al. Assessment of the quality of TROPOMI high-spatial-resolution NO₂ data products in the Greater Toronto Area. *Atmos. Meas. Tech.* **2020**, *13*, 2131–2159. [CrossRef]
51. Williams, J.E.; Boersma, K.F.; Le Sager, P.; Verstraeten, W.W. The high-resolution version of TM5-MP for optimized satellite retrievals: Description and validation. *Geosci. Model Dev.* **2017**, *10*, 721–750. [CrossRef]
52. Rolph, G.; Stein, A.; Stunder, B. Real-time Environmental Applications and Display sYstem: READY. *Environ. Model. Softw.* **2017**, *95*, 210–228. [CrossRef]
53. Cui, L.; Song, X.; Zhong, G. Comparative Analysis of Three Methods for HYSPLIT Atmospheric Trajectories Clustering. *Atmosphere* **2021**, *12*, 698. [CrossRef]
54. Stein, A.F.; Draxler, R.R.; Rolph, G.D.; Stunder, B.J.B.; Cohen, M.D.; Ngan, F. NOAA's Hysplit Atmospheric Transport and Dispersion Modeling System. *Bull. Am. Meteorol. Soc.* **2015**, *96*, 2059–2078. [CrossRef]
55. Tyson, P.D. Atmospheric transport of aerosols and trace gases over southern Africa. *Prog. Phys. Geogr. Earth Environ.* **1997**, *21*, 79–101. [CrossRef]
56. Lourens, A.S.; Beukes, J.P.; Van Zyl, P.G.; Fourie, G.D.; Burger, J.W.; Pienaar, J.J.; Read, C.E.; Jordaan, J.H. Spatial and temporal assessment of gaseous pollutants in the highveld of South Africa. *S. Afr. J. Sci.* **2011**, *107*, 8. [CrossRef]
57. De Souza, A.; Aristone, F.; Abreu, M.C.; De Oliveira-Júnior, J.F.; Fernandes, W.A.; Pobocikova, I. Spatio-temporal variations of tropospheric nitrogen dioxide in South Mato Grosso based on remote sensing by satellite. *Meteorol. Atmos. Phys.* **2022**, *134*, 19. [CrossRef]
58. Tyson, P.D.; Garstang, M.; Swap, R. Large-Scale Recirculation of Air over Southern Africa. *J. Appl. Meteorol.* **1996**, *35*, 2218–2236. [CrossRef]
59. Thoithi, W.; Blamey, R.C.; Reason, C.J.C. Dry Spells, Wet Days, and Their Trends across Southern Africa during the Summer Rainy Season. *Geophys. Res. Lett.* **2021**, *48*, e2020GL091041. [CrossRef]
60. Mpungose, N.; Thoithi, W.; Blamey, R.C.; Reason, C.J.C. Extreme rainfall events in southeastern Africa during the summer. *Theoretical Appl. Climatol.* **2022**, *150*, 185–201. [CrossRef]
61. Kai, R.F.; Scholes, M.; Piketh, S.J.; Scholes, R.J. Analysis of the first surface nitrogen dioxide concentration observations over the South African Highveld derived from the Pandora-2s instrument. *Clean Air J.* **2022**, *32*, 1–11. [CrossRef]
62. Venter, A.; Lourens, A.S.M. Ambient air quality data reported at Sasol Secunda monitoring stations during COVID-19 lockdown—Mpumalanga, South Africa. *Clean Air J.* **2021**, *31*, 1–7. [CrossRef]
63. Tyson, P.D.; Garstang, M.; Swap, R.; Källberg, P.; Edwards, M. An Air Transport Climatology for Subtropical Southern Africa. *Int. J. Climatol.* **1996**, *16*, 265–291. [CrossRef]
64. Ibebuchi, C.C. Circulation pattern controls of wet days and dry days in Free State, South Africa. *Meteorol. Atmos. Phys.* **2021**, *133*, 1469–1480. [CrossRef]

65. Tyson, P.D.; Preston-Whyte, R.A. *The Weather and Climate of Southern Africa*; Oxford University Press: Oxford, UK, 2000.
66. Zhao, X.; Griffin, D.; Fioletov, V.; McLinden, C.; Davies, J.; Ogyu, A.; Lee, S.C.; Lupu, A.; Moran, M.D.; Cede, A.; et al. Retrieval of total column and surface NO₂ from Pandora zenith-sky measurements. *Atmos. Chem. Phys.* **2019**, *19*, 10619–10642. [[CrossRef](#)]
67. de Lange, A.; Naidoo, M.; Garland, R.M.; Dyson, L.L. The sensitivity of simulated surface-level pollution concentrations to WRF-ARW-model PBL parameterisation schemes over the Highveld of South Africa. *Atmos. Res.* **2021**, *254*, 105517. [[CrossRef](#)]
68. Rorich, R.P.; Galpin, J.S. Air quality in the Mpumalanga Highveld region, South Africa. *S. Afr. J. Sci.* **1998**, *94*, 109–114.
69. Cosijn, C. Stable discontinuities in the atmosphere over South Africa. *S. Afr. J. Sci.* **1996**, *92*, 381–386.
70. Hobbs, P.V. Clean air slots amid dense atmospheric pollution in southern Africa. *J. Geophys. Res. Atmos.* **2003**, *108*, 8490. [[CrossRef](#)]
71. Scholes, R.J.; Kendall, J.; Justice, C.O. The quantity of biomass burned in southern Africa. *J. Geophys. Res. Atmos.* **1996**, *101*, 23667–23676. [[CrossRef](#)]
72. Nkosi, C.; Piketh, S.; Burger, R.; Annegarn, H. Variability of domestic burning habits in the South African Highveld: A case study in the KwaDela Township (April 2017). In Proceedings of the 2017 International Conference on the Domestic Use of Energy (DUE), Cape Town, South Africa, 4–5 April 2017; pp. 23–29. [[CrossRef](#)]
73. Garstang, M.; Tyson, P.D.; Swap, R.; Edwards, M.; Kållberg, P.; Lindsay, J.A. Horizontal and vertical transport of air over southern Africa. *J. Geophys. Res. Atmos.* **1996**, *101*, 23721–23736. [[CrossRef](#)]
74. Tyson, P.D.; D’Abreton, P.C. Transport and recirculation of aerosols off Southern Africa—Macroscale plume structure. *Atmos. Environ.* **1998**, *32*, 1511–1524. [[CrossRef](#)]
75. Andreae, M.O.; Merlet, P. Emission of trace gases and aerosols from biomass burning. *Glob. Biogeochem. Cycles* **2001**, *15*, 955–966. [[CrossRef](#)]

Disclaimer/Publisher’s Note: The statements, opinions and data contained in all publications are solely those of the individual author(s) and contributor(s) and not of MDPI and/or the editor(s). MDPI and/or the editor(s) disclaim responsibility for any injury to people or property resulting from any ideas, methods, instructions or products referred to in the content.